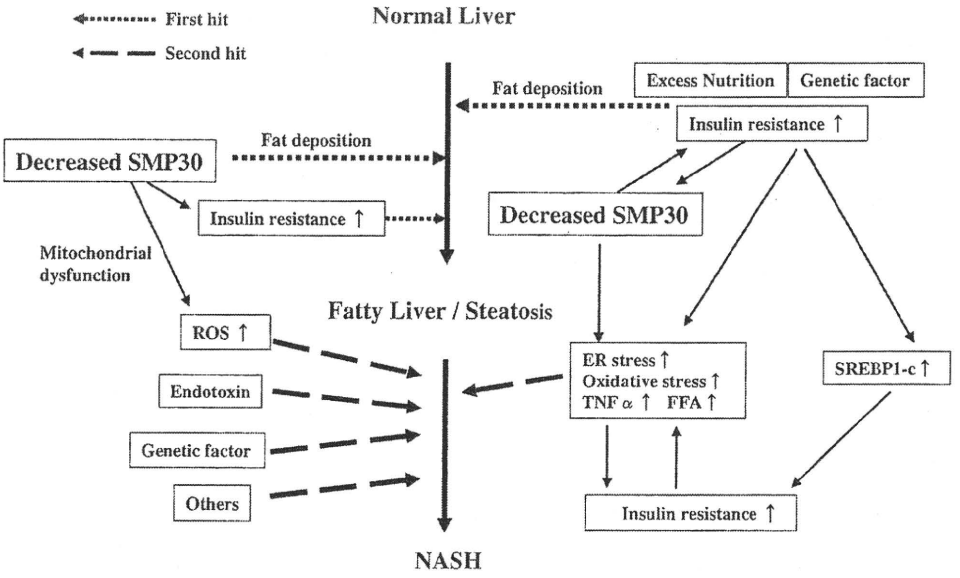

Fig. 6 Schematic diagram depicting disease progression of NAFLD according to the two-hit hypothesis, showing involvement of hepatic SMP30. *FFA*, free fatty acid; *SREBP*, sterol regulatory element-binding proteins; *TNF*, tumor necrosis factor

that steadily decreasing hepatic SMP30 levels are associated with the progression of hepatic insulin resistance.

In conclusion, the two-hit theory proposed by Day and James [9], in which the initial trigger is the hepatic accumulation of excessive fat, followed by the second hit of the development of oxidative stress, is widely advocated as a pathogenic mechanism for NASH. Therefore, our findings in the present study strongly suggest that SMP30 plays an important role in the pathogenesis of NAFLD (Fig. 6), and that increasing levels of SMP30 in the liver will serve as a promising target in the treatment of NASH.

Acknowledgments This study was supported by a Grant-in-Aid for Scientific Research (C) from the Japan Society for the Promotion of Science (Goji Hasegawa), and a Grant-in-Aid from the Ministry of Health, Labour and Welfare (Takeshi Okanoue).

References

1. Angulo P. Nonalcoholic fatty liver disease. N Engl J Med. 2002;18:1221–31.
2. Browning JD, Szczepaniak LS, Dobbins R, Nuremberg P, Horton JD, Cohen JC, et al. Prevalence of hepatic steatosis in an urban population in the United States: impact of ethnicity. Hepatology. 2004;40:1387–95.
3. Farrell GC. Non-alcoholic steatohepatitis: what is it, and why is it important in the Asia-Pacific region? J Gastroenterol Hepatol. 2003;18:124–38.
4. Ludwig J, Viggiano TR, McGill DB, Oh BJ. Nonalcoholic steatohepatitis: Mayo Clinic experiences with a hitherto unnamed disease. Mayo Clin Proc. 1980;55:434–8.
5. Kleiner DE, Brunt EM, Van Natta M, Behling C, Contos MJ, Cummings OW, et al. Design and validation of a histological scoring system for nonalcoholic fatty liver disease. Hepatology. 2005;41:1313–21.
6. Brunt EM, Janney CG, Di Bisceglie AM, Neuschwander-Tetri BA, Bacon BR. Nonalcoholic steatohepatitis: a proposal for grading and staging the histological lesions. Am J Gastroenterol. 1999;94:2467–74.
7. Chitturi S, Abeygunasekera S, Farrell GC, Holmes-Walker J, Hui JM, Fung C, et al. NASH and insulin resistance: Insulin hypersecretion and specific association with the insulin resistance syndrome. Hepatology. 2002;35:373–9.
8. Sanyal AJ, Campbell-Sargent C, Mirshahi F, Rizzo WB, Contos MJ, Sterling RK, et al. Nonalcoholic steatohepatitis: association of insulin resistance and mitochondrial abnormalities. Gastroenterology. 2001;120:1183–92.
9. Day CP, James OF. Steatohepatitis: a tale of two "hits"? Gastroenterology. 1998;114:842–5.
10. Fujita T, Uchida K, Maruyama N. Purification of senescence marker protein-30 (SMP30) and its androgen-independent decrease with age in the rat liver. Biochim Biophys Acta. 1992; 1116:122–8.
11. Ishigami A, Maruyama N. Significance of SMP30 in gerontology. Geriatr Gerontol Int. 2007;7:316–25.
12. Fujita T, Inoue H, Kitamura T, Sato N, Shimosawa T, Maruyama N. Senescence marker protein-30 (SMP30) rescues cell death by enhancing plasma membrane Ca(2+)-pumping activity in Hep G2 cells. Biochem Biophys Res Commun. 1998;250:374–80.
13. Inoue H, Fujita T, Kitamura T, Shimosawa T, Nagasawa R, Inoue R, et al. Senescence marker protein-30 (SMP30) enhances the calcium efflux from renal tubular epithelial cells. Clin Exp Nephrol. 1999;3:261–7.
14. Kondo Y, Inai Y, Sato Y, Handa S, Kubo S, Shimokado K, et al. Senescence marker protein 30 functions as gluconolactonase in L-ascorbic acid biosynthesis, and its knockout mice are prone to scurvy. Proc Natl Acad Sci USA. 2006;103:5723–8.
15. Ishigami A, Fujita T, Handa S, Shirasawa T, Koseki H, Kitamura T, et al. Senescence marker protein-30 knockout mouse liver is highly susceptible to tumor necrosis factor-alpha- and Fas-mediated apoptosis. Am J Pathol. 2002;161:1273–81.
16. Ishigami A, Kondo Y, Nanba R, Ohsawa T, Handa S, Kubo S, et al. SMP30 deficiency in mice causes an accumulation of neutral lipids and phospholipids in the liver and shortens the life span. Biochem Biophys Res Commun. 2004;315:575–80.
17. Sato T, Seyama K, Sato Y, Mori H, Souma S, Akiyoshi T, et al. Senescence marker protein-30 protects mice lungs from oxidative stress, aging, and smoking. Am J Respir Crit Care Med. 2006; 174:530–7.

18. Son TG, Zou Y, Jung KJ, Yu BP, Ishigami A, Maruyama N, et al. SMP30 deficiency causes increased oxidative stress in brain. Mech Ageing Dev. 2006;127:451–7.
19. Kondo Y, Sasaki T, Sato Y, Amano A, Aizawa S, Iwama M, et al. Vitamin C depletion increases superoxide generation in brains of SMP30/GNL knockout mice. Biochem Biophys Res Commun. 2008;377:291–6.
20. Sato Y, Kajiyama S, Amano A, Kondo Y, Sasaki T, Handa S, et al. Hydrogen-rich pure water prevents superoxide formation in brain slices of vitamin C-depleted SMP30/GNL knockout mice. Biochem Biophys Res Commun. 2008;375:346–50.
21. Okazaki M, Usui S, Ishigami M, Sakai N, Nakamura T, Matsuzawa Y, et al. Identification of unique lipoprotein subclasses for visceral obesity by component analysis of cholesterol profile in high-performance liquid chromatography. Arterioscler Thromb Vasc Biol. 2005;25:578–84.
22. Okazaki M, Usui S, Fukui A, Kubota I, Tomoike H. Component analysis of HPLC profiles of unique lipoprotein subclass cholesterols for detection of coronary artery disease. Clin Chem. 2006;52:2049–53.
23. Poli G. Pathogenesis of liver fibrosis: role of oxidative stress. Mol Aspects Med. 2000;21:49–98.
24. Matsuoka M, Tsukamoto H. Stimulation of hepatic lipocyte collagen production by Kupffer cell-derived transforming growth factor beta: implication for a pathogenetic role in alcoholic liver fibrogenesis. Hepatology. 1990;11:599–605.
25. Tomita K, Oike Y, Teratani T, Taguchi T, Noguchi M, Suzuki T, et al. Hepatic AdipoR2 signaling plays a protective role against progression of nonalcoholic steatohepatitis in mice. Hepatology. 2008;48:458–73.
26. Parola M, Pinzani M, Casini A, Albano E, Poli G, Gentilini A, et al. Stimulation of lipid peroxidation or 4-hydroxynonenal treatment increases procollagen alpha 1 (I) gene expression in human liver fat-storing cells. Biochem Biophys Res Commun. 1993;194:1044–50.
27. Parola M, Pinzani M, Casini A, Leonarduzzi G, Marra F, Caligiuri A, et al. Induction of procollagen type I gene expression and synthesis in human hepatic stellate cells by 4-hydroxy-2,3-nonenal and other 4-hydroxy-2,3-alkenals is related to their molecular structure. Biochem Biophys Res Commun. 1996;222:261–4.
28. Park JK, Jeong DH, Park HY, Son KH, Shin DH, Do SH, et al. Hepatoprotective effect of Arazyme on CCl4-induced acute hepatic injury in SMP30 knock-out mice. Toxicology. 2008;246:132–42.
29. Jeong DH, Goo MJ, Hong IH, Yang HJ, Ki MR, Do SH, et al. Inhibition of radiation-induced apoptosis via overexpression of SMP30 in Smad3-knockout mice liver. J Radiat Res (Tokyo). 2008;49:653–60.
30. Griffin BA, Packard CJ. Metabolism of VLDL and LDL subclasses. Curr Opin Lipidol. 1994;5:200–6.
31. Packard CJ. Triacylglycerol-rich lipoproteins and the generation of small, dense low-density lipoprotein. Biochem Soc Trans. 2003;31(Pt 5):1066–9.
32. Adiels M, Borén J, Caslake MJ, Stewart P, Soro A, Westerbacka J, et al. Overproduction of VLDL1 driven by hyperglycemia is a dominant feature of diabetic dyslipidemia. Arterioscler Thromb Vasc Biol. 2005;25:1697–703.
33. Adiels M, Taskinen MR, Packard C, Caslake MJ, Soro-Paavonen A, Westerbacka J, et al. Overproduction of large VLDL particles is driven by increased liver fat content in man. Diabetologia. 2006;49:755–65.

ELSEVIER

Cancer Genetics and Cytogenetics 198 (2010) 118–125

CANCER GENETICS AND CYTOGENETICS

PEG10 is a probable target for the amplification at 7q21 detected in hepatocellular carcinoma

Kazuhiro Tsuji[a], Kohichiroh Yasui[a,*], Yasuyuki Gen[a], Mio Endo[a], Osamu Dohi[a], Keika Zen[a], Hironori Mitsuyoshi[a], Masahito Minami[a], Yoshito Itoh[a], Masafumi Taniwaki[b], Shinji Tanaka[c], Shigeki Arii[c], Takeshi Okanoue[a,d], Toshikazu Yoshikawa[a]

[a]*Department of Molecular Gastroenterology and Hepatology, Graduate School of Medical Science, Kyoto Prefectural University of Medicine, 465 Kajii-cho, Kamigyo-ku, Kyoto 602-8566, Japan*

[b]*Department of Molecular Hematology and Oncology, Graduate School of Medical Science, Kyoto Prefectural University of Medicine, Kyoto, Japan*

[c]*Department of Hepato-Biliary-Pancreatic Surgery, Tokyo Medical and Dental University, Tokyo, Japan*

[d]*Center of Gastroenterology and Hepatology, Saiseikai Suita Hospital, Suita, Osaka, Japan*

Received 3 September 2009; received in revised form 3 January 2010; accepted 3 January 2010

Abstract DNA copy number aberrations in human hepatocellular carcinoma (HCC) cell lines were investigated using a high-density oligonucleotide microarray, and a novel amplification at the chromosomal region 7q21 was detected. Molecular definition of the amplicon indicated that *PEG10* (paternally expressed gene 10), a paternally expressed imprinted gene, was amplified together with *CDK14* (cyclin-dependent kinase 14; previously PFTAIRE protein kinase 1, *PFTK1*) and *CDK6* (cyclin-dependent kinase 6). An increase in *PEG10* copy number was detected in 14 of 34 primary HCC tumors (41%). *PEG10*, but not *CDK14* or *CDK6*, was significantly overexpressed in 30 of 41 tumors (73%) from HCC patients, compared with their nontumorous counterparts. These results suggest that *PEG10* is a probable target, acting as a driving force for amplification of the 7q21 region, and may therefore be involved in the development or progression of HCCs.

1. Introduction

Hepatocellular carcinoma (HCC) is the fifth most common malignancy in men and the eighth most common in women worldwide; it is estimated to cause approximately half a million deaths annually [1]. Although the risk factors for HCC, which include hepatitis B virus, hepatitis C virus, and alpha-toxin, are well characterized, the molecular pathogenesis of this widespread type of cancer remains poorly understood [2].

Amplification of DNA in certain regions of chromosomes plays a crucial role in the development and progression of human malignancies, specifically when protooncogenic target genes within those amplicons are overexpressed. Oncogenes that are often amplified in cancers include *MYC*, *ERBB2*, and *CCND1*. The recent introduction of high-density oligonucleotide microarrays designed for typing of single nucleotide polymorphisms (SNPs) facilitates high-resolution mapping of chromosomal amplifications, deletions, and losses of heterozygosity [3,4].

To identify genes potentially involved in HCC, we investigated DNA copy number aberrations in human HCC cell lines using high-resolution SNP arrays and found a novel amplification at the chromosomal region 7q21. Recurrent amplifications at 7q21 have been observed in human neoplasms [5]. Gains of 7q21 have been associated with the aggressiveness of several tumors, including HCC [6], colorectal cancer [7], prostate cancer [8], Burkitt lymphoma [9], and esophageal squamous cell carcinoma [10]. These data suggest that this chromosomal region may harbor one or more protooncogenes (henceforth referred to as *target genes*) whose overexpression following amplification might contribute to the initiation or progression of HCC. The actual target gene that drives the 7q21 amplification in HCC remains unclear, however, and we therefore conducted a molecular definition study of the amplicon to identify such genes. Three putative oncogenes, *CDK14* (cyclin-dependent kinase 14; previously *PFTK1*, PFTAIRE protein kinase 1), *CDK6* (cyclin-dependent

* Corresponding author. Tel.: +81-75-251-5519; fax: +81-75-251-0710.

E-mail address: yasuik@koto.kpu-m.ac.jp (K. Yasui).

0165-4608/10/$ – see front matter
doi:10.1016/j.cancergencyto.2010.01.004

kinase 6), and *PEG10* (paternally expressed gene 10), were identified in the 7q21 amplicon.

The serine/threonine-protein kinase PFTAIRE-1 protein (also known as PFTK1) is a member of the cell division cycle-2 (CDC2)-related protein kinase family [11] and acts as a cyclin-dependent kinase that regulates cell cycle progression and cell proliferation [12]. CDK6 is activated in response to increased expression of D-type cyclins in the early G1 phase of the cell cycle and inactivates the retinoblastoma protein by phosphorylation, thereby activating the transcriptional complex E2F-DP1 that regulates the genes for S-phase onset [13]. *PEG10* has been characterized as a paternally expressed, maternally silenced gene [14]. Several research groups have recently reported overexpression of *PEG10* in HCC [15–19].

2. Materials and methods

2.1. Cell lines and tumor samples

A total of 20 HCC cell lines were examined: JHH-1, JHH-2, JHH-4, JHH-5, JHH-6, JHH-7, SNU354, SNU368, SNU387, SNU398, SNU423, SNU449, SNU475, Huh-1, Huh7, Hep3B, PLC/PRF/5, Li7, HLE, and HLF [20]. All cell lines were maintained in Dulbecco's modified Eagle's medium supplemented with 10% fetal calf serum. Paired tumor and nontumor tissues were obtained from 36 HCC patients who underwent surgery at the Hospital of Tokyo Medical and Dental University. All specimens were frozen immediately in liquid nitrogen and were stored at −80°C until required. Genomic DNA was isolated using a Puregene DNA isolation kit (Gentra, Minneapolis, MN), and total RNA was obtained using Trizol reagent (Invitrogen, Carlsbad, CA). Thirty-four tumor samples were available for DNA analyses, and 41 paired tumor and nontumor samples were available for mRNA analyses.

Prior to the study, informed consent was obtained and the study was approved by ethics committees.

2.2. SNP array analysis

DNA copy number changes were analyzed by the GeneChip Mapping 100K array set (Affymetrix, Santa Clara, CA) according to the manufacturer's instructions as described previously [21]. In brief, 250 ng of genomic DNA was digested with a restriction enzyme (*Xba*I or *Hin*dIII), ligated to an adaptor and amplified by polymerase chain reaction (PCR). Amplified products were fragmented, labeled by biotinylation, and hybridized to the microarrays. Hybridization was detected by incubation with a streptavidin–phycoerythrin conjugate, followed by scanning of the array; analysis was performed as previously described [22]. After appropriate normalization of mean array intensities, signal ratios were calculated between HCC cell lines and anonymous normal references, and copy numbers were inferred from the observed signal ratios based on the hidden Markov model using CNAG software (Copy Number Analyzer for Affymetrix GeneChip mapping arrays) [23]. The CNAG software is available at http://www.genome.umin.jp.

2.3. Fluorescence in situ hybridization

Fluorescence in situ hybridization (FISH) was performed using five bacterial artificial chromosomes (BACs) as probes, as described previously [24]: RP11-66P5, RP11-412F4, RP11-316P4, RP11-28O23, and RP11-958G24 (Invitrogen, Carlsbad, CA). The BACs were selected based on their homology to locations in the human genome according to the database provided at the University of California, Santa Cruz, Genome Bioinformatics Web site (http://genome.ucsc.edu/).

2.4. Real-time quantitative PCR

Genomic DNA and mRNA were quantified using a real-time fluorescence detection method, as described previously [21]. The primers used for PCR (Table 1) were designed using Primer3Plus software (http://www.bioinformatics.nl/cgi-bin/primer3plus/primer3plus.cgi) on the basis of sequence data obtained from the National Center for Biotechnology Information (http://www.ncbi.nlm.nih.gov/) database. *GAPDH* was used as endogenous control for mRNA levels, and the long interspersed nuclear element 1 (LINE-1) was used as an endogenous control for genomic DNA levels.

2.5. Statistical analysis

The Wilcoxon signed-rank test was performed using SPSS 15.0 software (SPSS, Chicago, IL). P values of <0.05 were considered significant.

Table 1
Primer sequences used for polymerase chain reaction with sequence-tagged site (STS) markers for the three genes investigated

Gene	STS marker	Forward primer	Reverse primer
CDK14 genomic DNA	D7S627	5′-AAACCAAGAACATTCCAG-3′	5′-ACACATCACATTCTCACC-3′
CDK14 mRNA		5′-CCAAGGAGTTGCTGCTTTTC-3′	5′-GAATGAACTCCAGGCCATGT-3′
CDK6 genomic DNA	SHGC-33519	5′-AAGTCAGAAGGAAAAAAGCTTACTG-3′	5′-TGAGATGTGTTAAAGTAGGTTTTCA-3′
CDK6 mRNA		5′AGCCCAAGATGACCAACATC-3′	5′-AGGTCAAGTTGGGAGTGGTG-3′
PEG10 genomic DNA	STS-H51766	5′-AAAGTTTACATACATTTATGAAGGG-3′	5′- TTCCAGACTGCACCATATAG-3′
PEG10 mRNA		5′-CAGGCCTGAAAAGAAAGTGC-3′	5′-AATGCTTTGTGGAAGCCATC-3′

The gene *CDK14* was previously assigned the symbol *PFTK1* (http://www.genenames.org).

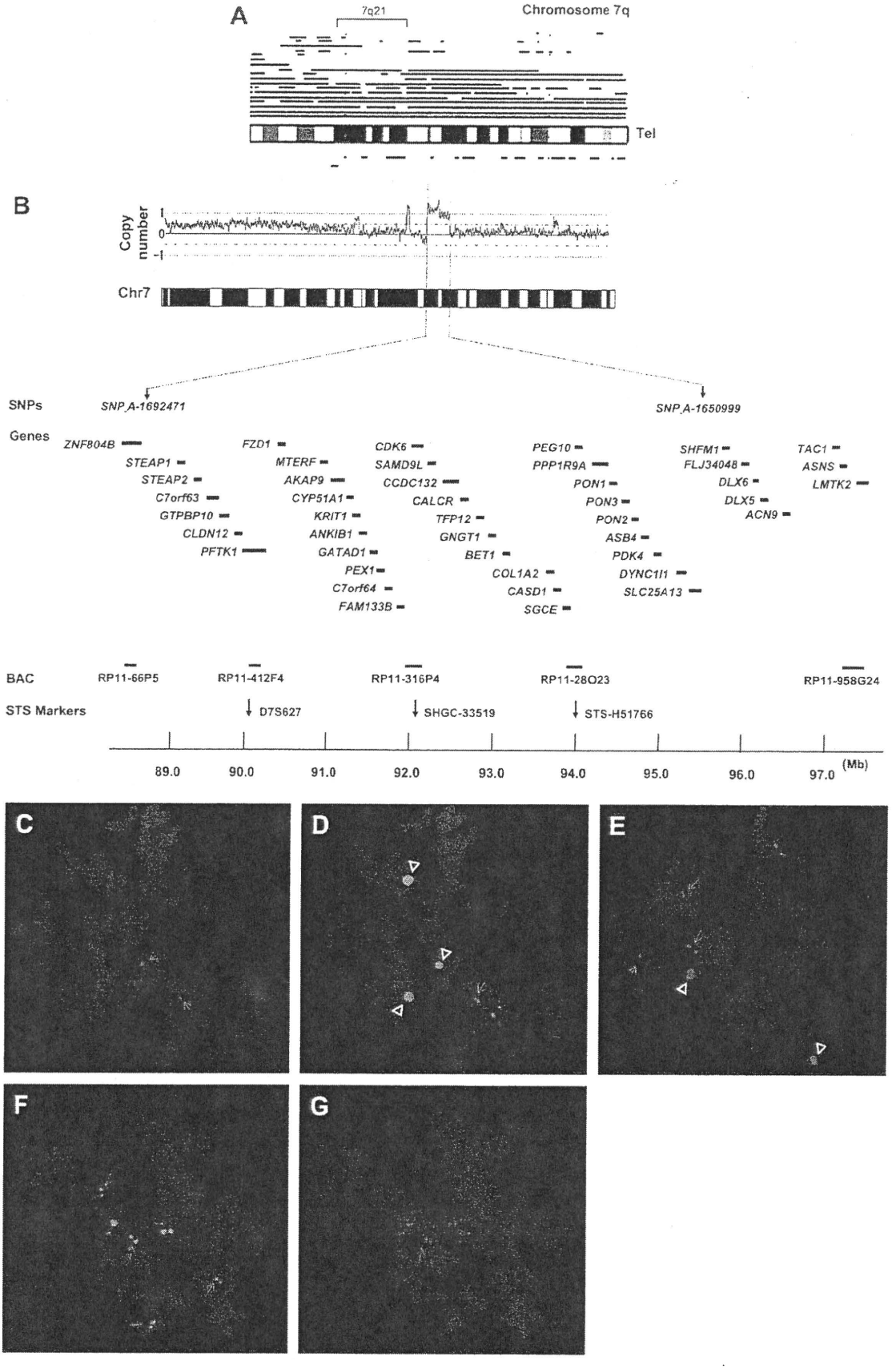
A
7q21
Chromosome 7q
Tel
B
Copy number
Chr7
SNPs
SNP_A-1692471
SNP_A-1650999
Genes
ZNF804B
STEAP1
STEAP2
C7orf63
GTPBP10
CLDN12
PFTK1
FZD1
MTERF
AKAP9
CYP51A1
KRIT1
ANKIB1
GATAD1
PEX1
C7orf64
FAM133B
CDK6
SAMD9L
CCDC132
CALCR
TFP12
GNGT1
BET1
COL1A2
CASD1
SGCE
PEG10
PPP1R9A
PON1
PON3
PON2
ASB4
PDK4
DYNC1I1
SLC25A13
SHFM1
FLJ34048
DLX6
DLX5
ACN9
TAC1
ASNS
LMTK2
BAC
RP11-66P5
RP11-412F4
RP11-316P4
RP11-28O23
RP11-958G24
STS Markers
D7S627
SHGC-33519
STS-H51766
89.0
90.0
91.0
92.0
93.0
94.0
95.0
96.0
97.0
(Mb)
C
D
E
F
G

3. Results

3.1. Detection of the 7q21 amplicon

Twenty HCC cell lines were screened for DNA copy number aberrations by GeneChip Mapping 100K array analysis. The copy number detection algorithm CNAG allowed assessment of copy number and identification of genomic gains and deletions using the hidden Markov model [23]. Gains at the chromosomal region 7q21 were frequently found in 13 of the 20 cell lines (65%) (Fig. 1A). Of these cell lines, JHH-4 cells exhibited a high-level copy number gain indicative of gene amplification at 7q21 (Fig. 1B). The estimated extent of the amplification in JHH-4 cells is 9 Mb. This chromosomal region lies between the Affymetrix markers SNP_A-1692471 and SNP_A-1650999 (supplementary Table S1) and includes 35 known or predicted protein-coding genes. The 7q21 region may harbor one or more genes that, when activated by amplification, play a role in carcinogenesis. Because we identified three putative oncogenes (i.e., *CDK14*, *CDK6*, and *PEG10*) in the 7q21 amplicon, we chose to focus further analysis on these three genes.

To confirm amplification of *CDK14*, *CDK6*, and *PEG10*, we performed FISH analyses on JHH-4 cells using the BACs RP11-66p5, RP11-412F4, RP11-316P4, RP11-28O23, and RP11-958G24 as probes. RP11-412F4 (containing *CDK14*) (Fig. 1D) and RP11-316P4 (containing *CDK6*) (Fig. 1E) generated amplified FISH signals, and RP11-28O23 (containing *PEG10*) (Fig. 1F) showed an increase in the number of FISH signals. In contrast, neither RP11-66P5 nor RP11-958G24, which correspond to chromosomal regions outside of the amplicon, showed an amplified signal or an increase in the number of FISH signals (Fig. 1C, 1G). These data confirm that *CDK14*, *CDK6*, and *PEG10* are amplified in JHH-4 cells.

3.2. DNA copy number and expression level of CDK14, CDK6, and PEG10 in HCC cell lines

To further analyze the potential role of *CDK14*, *CDK6*, and *PEG10* in HCC, we determined the DNA copy number of these three genes in 20 HCC cell lines by real-time quantitative PCR. For this analysis, copy number changes were counted as gains if the copy number for a given tumor cell type exceeded the mean plus 2 standard deviations of the level of the gene in normal cells. A copy number gain of *CDK14*, *CDK6*, and *PEG10* was observed in 13 (65%), 12 (60%), and 14 (70%) of the 20 cell lines, respectively (Fig. 2A). JHH-4 cells showed the highest copy number gain of each gene.

A common criterion for designation of a gene as a putative target of amplification is that gene amplification leads to its overexpression [25]. To determine whether *CDK14*, *CDK6*, and *PEG10* are overexpressed, we determined the mRNA level of these three genes in the 20 HCC cell lines by real-time quantitative PCR. Both *CDK6* and *PEG10*, but not *CDK14*, were overexpressed in JHH-4 cells, relative to the other cell lines (Fig. 2B). These findings suggested that *CDK6* and *PEG10* are candidate targets for the 7q21 amplification.

3.3. DNA copy number and expression level of CDK14, CDK6, and PEG10 in primary HCC tumors

To determine whether the amplification of *CDK14*, *CDK6*, and *PEG10* that was observed in JHH-4 cells was relevant to primary human carcinomas, we first determined the copy number of the three genes in 34 primary HCCs, using a method similar to that used for the HCC cell lines. A copy number gain of *CDK14*, *CDK6*, and *PEG10* was observed in 8 (24%), 16 (47%), and 14 (41%), respectively, of the 34 tumors (Fig. 3).

We then further examined the expression of the three genes in paired tumor and nontumor tissues from the 41 HCC patients by real-time quantitative PCR. Patient and tumor characteristics are summarized in Table 2. *PEG10* was significantly overexpressed in 30 of the 41 tumors (73%), compared with their nontumorous counterparts (Wilcoxon signed-rank test, $P < 0.001$) (Fig. 4). In contrast, expression of *CDK14* or *CDK6* was not upregulated in HCC tumors (Fig. 4). Taken together, these results suggest that *PEG10* is the most likely target for the 7q21 amplicon in HCC.

Fig. 1. Map of the amplicon at 7q21 in the human hepatocellular carcinoma (HCC) cell line JHH-4. (A) Recurrent copy number gains on the 7q arm as assessed using a GeneChip mapping 100K array (Affymetrix, Santa Clara, CA). Copy number gains are indicated by red horizontal lines above the chromosome ideogram: high-level gains (amplifications) are shown by bright red lines, whereas simple gains are shown by dark red lines. Copy number losses are indicated by green lines under the chromosome ideogram. Each horizontal line represents an aberration detected in a single HCC cell line. The cytobands in 7q are shown. (B) Copy number profile of chromosome 7 in JHH-4 cells. Copy number values were determined by GeneChip mapping 100K array analysis. Shown are the position of the Affymetrix single-nucleotide polymorphism (SNP) probes, the 35 genes included within the amplicon, the five bacterial artificial chromosomes (BACs) used as probes for fluorescence in situ hybridization (FISH) experiments, and the three sequence-tagged site (STS) markers used for real-time quantitative polymerase chain reaction (PCR) based on the University of California, Santa Cruz, Genome Bioinformatics database (http://genome.ucsc.edu/). (C-G) Representative images of FISH on metaphase chromosomes from JHH-4 cells, using the following BAC probes: paired RP11-66P5, containing *ZNF804B* (red) (C) and RP11-412F4, containing *CDK14* (green) (D); single RP11-316P4, containing *CDK6* (red) (E); and paired RP11-28O23, containing *PEG10* (green) (F) and RP11-958G24, containing *LMTK2* (red) (G). Arrows indicate normal signals; arrowheads indicate amplified signals. The set of images shows two normal signals (C), three amplified signals plus two normal signals (D), two amplified signals plus four normal signals (E), six normal signals (F), and three normal signals (G). *Note:* In these figures the gene *CDK14* is identified by the previously approved symbol, *PFTK1*.

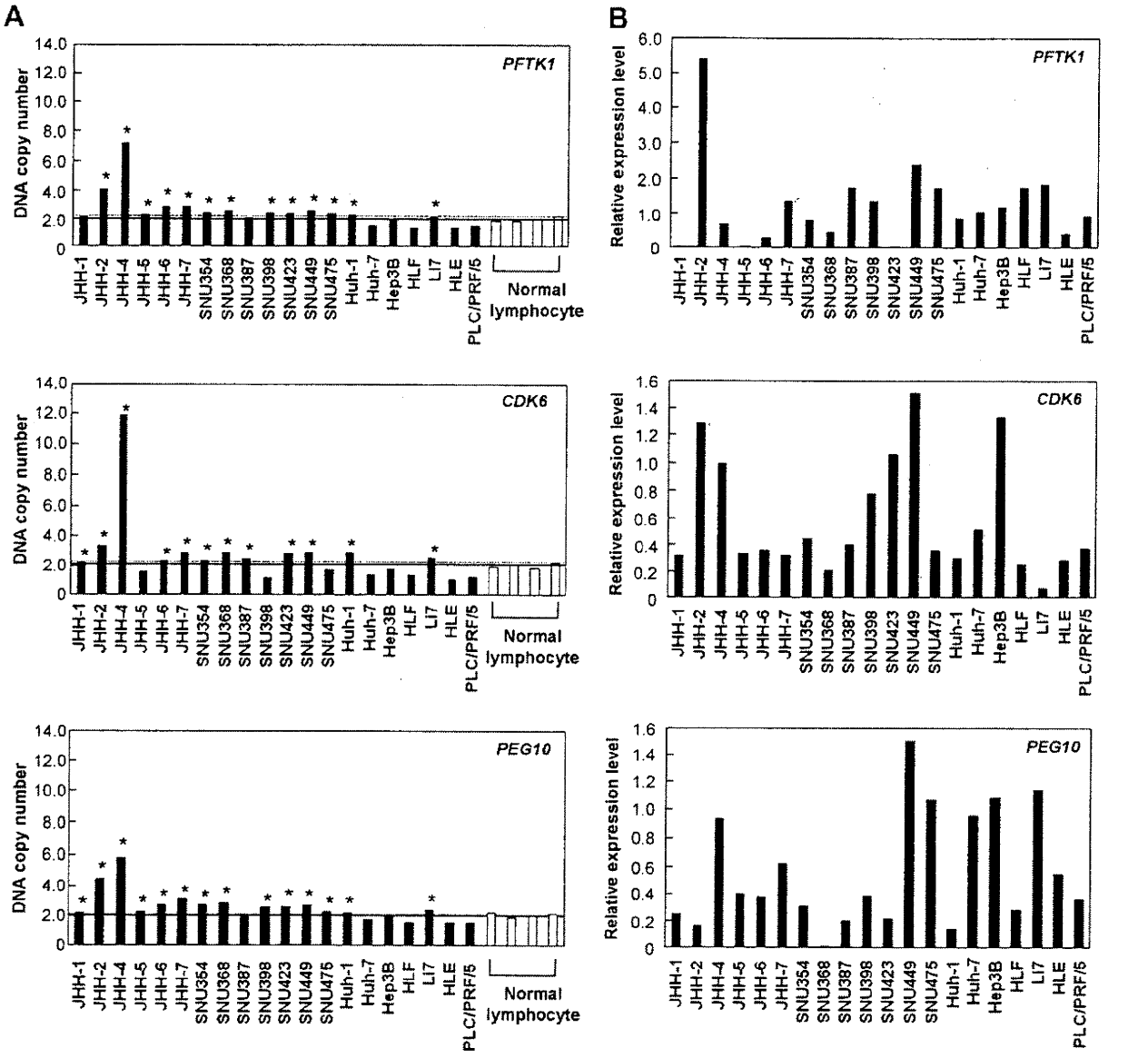

Fig. 2. DNA copy number and expression level of *CDK14* (previously *PFTK1*), *CDK6*, and *PEG10* in HCC cell lines. (A) DNA copy number of *CDK14*, *CDK6*, and *PEG10* in 20 HCC cell lines and four normal peripheral blood lymphocytes as measured by real-time quantitative PCR with reference to LINE-1 controls. Values are normalized such that the average copy number in genomic DNA derived from four normal lymphocytes has a value of 2 (solid horizontal line). A value corresponding to the mean +2 S.D. of the copy number of normal lymphocytes was used as the cutoff value for copy number gain (dotted line). Asterisks indicate cell lines showing copy number gain. (B) Relative expression levels of *CDK14*, *CDK6*, and *PEG10* in 20 HCC cell lines as determined by real-time quantitative PCR. The results are presented as the expression level of each gene relative to a reference gene (*GAPDH*), to correct for variations in the amount of RNA.

4. Discussion

The high-resolution SNP array analysis reported in this study identified amplification at the chromosomal region 7q21 in JHH-4 HCC cells. A copy number gain at this region was frequently observed, not only in HCC cell lines, but also in primary HCCs. Of the three genes identified in the amplicon (i.e., *PEG10*, *CDK6*, and *CDK14*), subsequent experiments suggested that *PEG10* is the most likely target for the amplicon, in that the *PEG10* transcript was both overexpressed in JHH-4 cells and significantly upregulated in primary HCC tumors, compared with their nontumorous counterparts. In contrast, although the highest level of copy number gain was found at the *CDK6* locus in JHH-4 cells and primary HCC tumors, *CDK6* expression was not upregulated in primary HCC tumors.

Contrary to these data, a recent report indicated that expression of *CDK14* was higher in HCC tumors than in

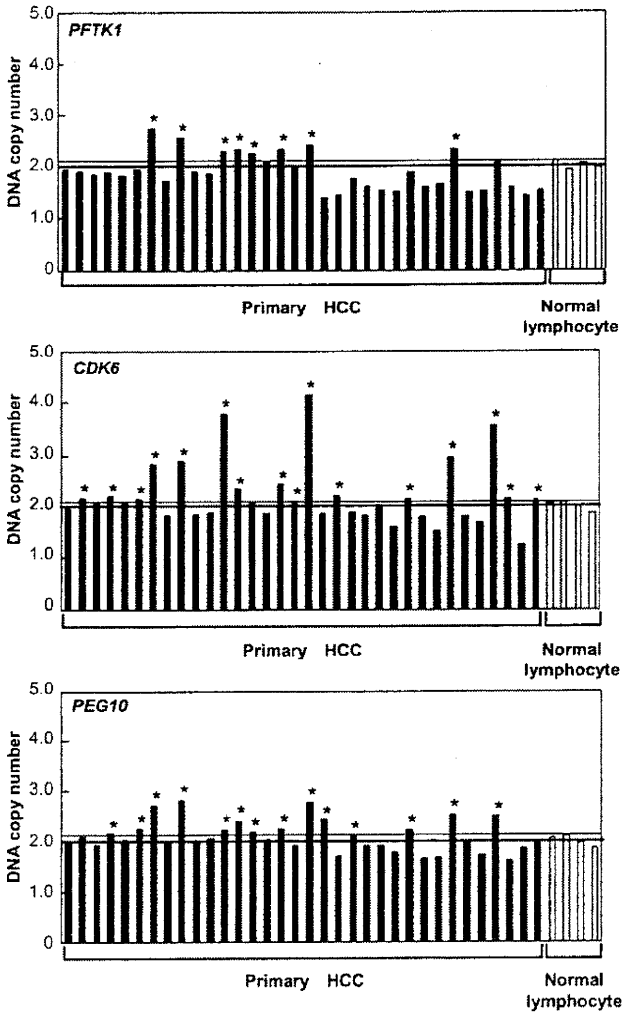

Fig. 3. DNA copy number of *CDK14* (previously *PFTK1*), *CDK6*, and *PEG10* in primary HCC tumors. The DNA copy number of each gene in 34 primary HCC tumors and four normal peripheral blood lymphocytes was determined as already described (for Fig. 2A). Asterisks indicate primary tumors showing copy number gain.

Table 2
Patient and tumor characteristics

Characteristics	Value[a]
Sample size[b]	$n = 41$
Sex	
Male	33
Female	8
Median age, yr (range)	67 (35–79)
Etiology of liver disease	
Hepatitis B virus	9
Hepatitis C virus	21
Other	11
Median tumor size, cm (range)	5.0 (1.9–26)
Tumors, single or multiple	
Single	26
Multiple	15
Tumor differentiation	
Well	7
Moderate	20
Poor	14
Stage[c]	
I	1
II	15
III	14
IV	11
Background liver tissue	
Normal	4
Chronic hepatitis	18
Liver cirrhosis	19
Child–Pugh classification	
A	40
B	1
C	0
Median α-fetoprotein, ng/mL (range)	14.9 (0.9–114,859)

[a] Where no other unit is specified, values refer to number of patients.
[b] All patients were of Japanese ethnicity.
[c] International Union Against Cancer tumor–node–metastasis (UICC TNM) classification of malignant tumor.

adjacent nontumorous liver tissues and that upregulation of the gene correlated with both advanced metastatic HCCs and microvascular invasion [26]. Further studies are required to clarify the potential role of *CDK14* in HCC.

PEG10 was first identified as an imprinted gene that is paternally expressed and maternally silenced [14]. It has been suggested that *PEG10* is derived from a retrotransposon that was previously integrated into the mammalian genome [14]. The overexpression of *PEG10* in HCC observed in this study is consistent with the previously reported overexpression of *PEG10* in tumors, including HCC [15–19], and in B-cell leukemia [27,28]. Furthermore, several lines of evidence suggest that *PEG10* may be important for the regulation of cell proliferation and cell death: *PEG10* is overexpressed in regenerating mouse liver [16], knockdown of *PEG10* inhibits the proliferation of cancer cells [29], and the PEG10 protein inhibits cell death mediated by SIAH1, a mediator of apoptosis [15]. The importance of *PEG10* for cell regulation is further suggested by the fact that targeted disruption of the mouse *Peg10* gene results in early embryonic lethality due to defects in the placenta [30].

The exact mechanism by which *PEG10* signals is unclear, but it is known to interact with members of the TGF-β receptor family [31]. Further evidence of a potential role for *PEG10* in cell growth and carcinogenesis is that its expression can be regulated by the protooncogene *MYC* [29], by E2F transcription factors that modulate the cell cycle [32], and by the sex hormone androgen [33].

Although the exact mechanism of *PEG10* function in tumors remains to be elucidated, and the findings in this study must be verified in future studies using a larger sample number, the data presented in this work suggest a role for amplification and overexpression of *PEG10* in hepatocarcinogenesis.

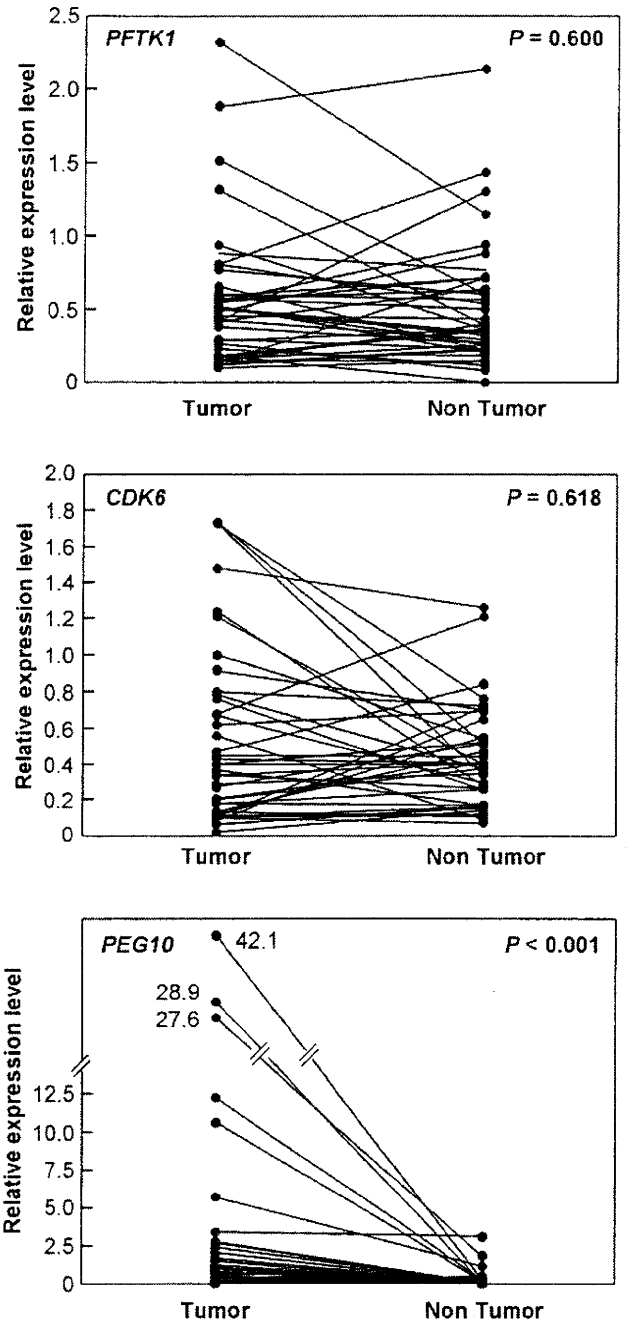

Fig. 4. Expression levels of *CDK14* (previously *PFTK1*), *CDK6*, and *PEG10* in paired tumor (T) and nontumor tissues (NT) from 41 patients with primary HCC. The expression level of each gene was determined as already described (for Fig. 2B). *CDK14*, *CDK6*, and *PEG10* were overexpressed in 22 (54%), 21 (51%), and 30 (73%) of the 41 tumors, respectively, compared with their nontumorous counterparts.

Acknowledgments

This work was supported by a Grant-in-Aid for Scientific Research (No. 20590408) from the Japan Society for the Program of Science (to K.Y.).

Supplementary data

Supplementary data associated with this article can be found, in the online version, at 10.1016/j.cancergencyto.2010.01.004.

References

[1] Bosch FX, Ribes J, Cléries R, Díaz M. Epidemiology of hepatocellular carcinoma. Clin Liver Dis 2005;9:191–211.
[2] Thorgeirsson SS, Grisham JW. Molecular pathogenesis of human hepatocellular carcinoma. Nat Genet 2002;31:339–46.
[3] Mei R, Galipeau PC, Prass C, Berno A, Ghandour G, Patil N, Wolff RK, Chee MS, Reid BJ, Lockhart DJ. Genome-wide detection of allelic imbalance using human SNPs and high-density DNA arrays. Genome Res 2000;10:1126–37.
[4] Zhao X, Li C, Paez JG, Chin K, Jänne PA, Chen TH, Girard L, Minna J, Christiani D, Leo C, Gray JW, Sellers WR, Meyerson M. An integrated view of copy number and allelic alterations in the cancer genome using single nucleotide polymorphism arrays. Cancer Res 2004;64:3060–71.
[5] Knuutila S, Björkqvist AM, Autio K, Tarkkanen M, Wolf M, Monni O, Szymanska J, Larramendy ML, Tapper J, Pere H, El-Rifai W, Hemmer S, Wasenius VM, Vidgren V, Zhu Y. DNA copy number amplifications in human neoplasms: review of comparative genomic hybridization studies. Am J Pathol 1998;152:1107–23.
[6] Sy SM, Wong N, Lai PB, To KF, Johnson PJ. Regional over-representations on chromosomes 1q, 3q and 7q in the progression of hepatitis B virus-related hepatocellular carcinoma. Mod Pathol 2005;18:686–92.
[7] Nakao K, Shibusawa M, Ishihara A, Yoshizawa H, Tsunoda A, Kusano M, Kurose A, Makita T, Sasaki K. Genetic changes in colorectal carcinoma tumors with liver metastases analyzed by comparative genomic hybridization and DNA ploidy. Cancer 2001;91:721–6.
[8] Strohmeyer DM, Berger AP, Moore DH 2nd, Bartsch G, Klocker H, Carroll PR, Loening SA, Jensen RH. Genetic aberrations in prostate carcinoma detected by comparative genomic hybridization and microsatellite analysis: association with progression and angiogenesis. Prostate 2004;59:43–58.
[9] García JL, Hernandez JM, Gutiérrez NC, Flores T, González D, Calasanz MJ, Martínez-Climent JA, Piris MA, Lopéz-Capitán C, González MB, Odero MD, San Miguel JF. Abnormalities on 1q and 7q are associated with poor outcome in sporadic Burkitt's lymphoma: a cytogenetic and comparative genomic hybridization study. Leukemia 2003;17:2016–24.
[10] Yen CC, Chen YJ, Chen JT, Hsia JY, Chen PM, Liu JH, Fan FS, Chiou TJ, Wang WS, Lin CH. Comparative genomic hybridization of esophageal squamous cell carcinoma: correlations between chromosomal aberrations and disease progression/prognosis. Cancer 2001;92:2769–77.
[11] Yang T, Chen JY. Identification and cellular localization of human PFTAIRE1. Gene 2001;267:165–72.
[12] Shu F, Lv S, Qin Y, Ma X, Wang X, Peng X, Luo Y, Xu BE, Sun X, Wu J. Functional characterization of human PFTK1 as a cyclin-dependent kinase. Proc Natl Acad Sci U S A 2007;104:9248–53.
[13] Sherr CJ, Roberts JM. CDK inhibitors: positive and negative regulators of G1-phase progression. Genes Dev 1999;13:1501–12.
[14] Ono R, Kobayashi S, Wagatsuma H, Aisaka K, Kohda T, Kaneko-Ishino T, Ishino F. A retrotransposon-derived gene, *PEG10*, is a novel imprinted gene located on human chromosome 7q21. Genomics 2001;73:232–7.
[15] Okabe H, Satoh S, Furukawa Y, Kato T, Hasegawa S, Nakajima Y, Yamaoka Y, Nakamura Y. Involvement of PEG10 in human hepatocellular carcinogenesis through interaction with SIAH1. Cancer Res 2003;63:3043–8.

[16] Tsou AP, Chuang YC, Su JY, Yang CW, Liao YL, Liu WK, Chiu JH, Chou CK. Overexpression of a novel imprinted gene, *PEG10*, in human hepatocellular carcinoma and in regenerating mouse livers. J Biomed Sci 2003;10:625–35.

[17] Jia HL, Ye QH, Qin LX, Budhu A, Forgues M, Chen Y, Liu YK, Sun HC, Wang L, Lu HZ, Shen F, Tang ZY, Wang XW. Gene expression profiling reveals potential biomarkers of human hepatocellular carcinoma. Clin Cancer Res 2007;13:1133–9.

[18] Ip WK, Lai PB, Wong NL, Sy SM, Beheshti B, Squire JA, Wong N. Identification of *PEG10* as a progression related biomarker for hepatocellular carcinoma. Cancer Lett 2007;250:284–91.

[19] Luo JH, Ren B, Keryanov S, Tseng GC, Rao UN, Monga SP, Strom S, Demetris AJ, Nalesnik M, Yu YP, Ranganathan S, Michalopoulos GK. Transcriptomic and genomic analysis of human hepatocellular carcinomas and hepatoblastomas. Hepatology 2006; 44:1012–24.

[20] Inagaki Y, Yasui K, Endo M, Nakajima T, Zen K, Tsuji K, Minami M, Tanaka S, Taniwaki M, Itoh Y, Arii S, Okanoue T. *CREB3L4*, *INTS3*, and *SNAPAP* are targets for the 1q21 amplicon frequently detected in hepatocellular carcinoma. Cancer Genet Cytogenet 2008;180:30–6.

[21] Zen K, Yasui K, Nakajima T, Zen Y, Zen K, Gen Y, Mitsuyoshi H, Minami M, Mitsufuji S, Tanaka S, Itoh Y, Nakanuma Y, Taniwaki M, Arii S, Okanoue T, Yoshikawa T. *ERK5* is a target for gene amplification at 17p11 and promotes cell growth in hepatocellular carcinoma by regulating mitotic entry. Genes Chromosomes Cancer 2009;48:109–20.

[22] Kennedy GC, Matsuzaki H, Dong S, Liu WM, Huang J, Liu G, Su X, Cao M, Chen W, Zhang J, Liu W, Yang G, Di X, Ryder T, He Z, Surti U, Phillips MS, Boyce-Jacino MT, Fodor SP, Jones KW. Large-scale genotyping of complex DNA. Nat Biotechnol 2003;21:1233–7.

[23] Nannya Y, Sanada M, Nakazaki K, Hosoya N, Wang L, Hangaishi A, Kurokawa M, Chiba S, Bailey DK, Kennedy GC, Ogawa S. A robust algorithm for copy number detection using high-density oligonucleotide single nucleotide polymorphism genotyping arrays. Cancer Res 2005;65:6071–9.

[24] Gen Y, Yasui K, Zen K, Nakajima T, Tsuji K, Endo M, Mitsuyoshi H, Minami M, Itoh Y, Tanaka S, Taniwaki M, Arii S, Okanoue T, Yoshikawa T. A novel amplification target, *ARHGAP5*, promotes cell spreading and migration by negatively regulating RhoA in Huh-7 hepatocellular carcinoma cells. Cancer Lett 2009;275:27–34.

[25] Collins C, Rommens JM, Kowbel D, Godfrey T, Tanner M, Hwang SI, Polikoff D, Nonet G, Cochran J, Myambo K, Jay KE, Froula J, Cloutier T, Kuo WL, Yaswen P, Dairkee S, Giovanola J, Hutchinson GB, Isola J, Kallioniemi OP, Palazzolo M, Martin C, Ericsson C, Pinkel D, Albertson D, Li WB, Gray JW. Positional cloning of *ZNF217* and *NABC1*: genes amplified at 20q13.2 and overexpressed in breast carcinoma. Proc Natl Acad Sci U S A 1998;95: 8703–8.

[26] Pang EY, Bai AH, To KF, Sy SM, Wong NL, Lai PB, Squire JA, Wong N. Identification of PFTAIRE protein kinase 1, a novel cell division cycle-2 related gene, in the motile phenotype of hepatocellular carcinoma cells. Hepatology 2007;46:436–45.

[27] Hu C, Xiong J, Zhang L, Huang B, Zhang Q, Li Q, Yang M, Wu Y, Wu Q, Shen Q, Gao Q, Zhang K, Sun Z, Liu J, Jin Y, Tan J. PEG10 activation by co-stimulation of CXCR5 and CCR7 essentially contributes to resistance to apoptosis in $CD19^{+}CD34^{+}$ B cells from patients with B cell lineage acute and chronic lymphocytic leukemia. Cell Mol Immunol 2004;1:280–94.

[28] Kainz B, Shehata M, Bilban M, Kienle D, Heintel D, Krömer-Holzinger E, Le T, Kröber A, Heller G, Schwarzinger I, Demirtas D, Chott A, Döhner H, Zöchbauer-Müller S, Fonatsch C, Zielinski C, Stilgenbauer S, Gaiger A, Wagner O, Jäger U. Overexpression of the paternally expressed gene 10 (*PEG10*) from the imprinted locus on chromosome 7q21 in high-risk B-cell chronic lymphocytic leukemia. Int J Cancer 2007;121:1984–93.

[29] Li CM, Margolin AA, Salas M, Memeo L, Mansukhani M, Hibshoosh H, Szabolcs M, Klinakis A, Tycko B. *PEG10* is a c-MYC target gene in cancer cells. Cancer Res 2006;66:665–72.

[30] Ono R, Nakamura K, Inoue K, Naruse M, Usami T, Wakisaka-Saito N, Hino T, Suzuki-Migishima R, Ogonuki N, Miki H, Kohda T, Ogura A, Yokoyama M, Kaneko-Ishino T, Ishino F. Deletion of *Peg10*, an imprinted gene acquired from a retrotransposon, causes early embryonic lethality. Nat Genet 2006;38:101–6.

[31] Lux A, Beil C, Majety M, Barron S, Gallione CJ, Kuhn HM, Berg JN, Kioschis P, Marchuk DA, Hafner M. Human retroviral *gag*- and *gag-pol*-like proteins interact with the transforming growth factor-β receptor activin receptor-like kinase 1. J Biol Chem 2005;280: 8482–93.

[32] Wang C, Xiao Y, Hu Z, Chen Y, Liu N, Hu G. PEG10 directly regulated by E2Fs might have a role in the development of hepatocellular carcinoma. FEBS Lett 2008;582:2793–8.

[33] Jie X, Lang C, Jian Q, Chaoqun L, Dehua Y, Yi S, Yanping J, Luokun X, Qiuping Z, Hui W, Feili G, Boquan J, Youxin J, Jinquan T. Androgen activates PEG10 to promote carcinogenesis in hepatic cancer cells. Oncogene 2007;26:5741–51.

Pathology International 2010; **60**: 175–183 doi:10.1111/j.1440-1827.2009.02504.x

Original Article

Nuclear size measurement is a simple method for the assessment of hepatocellular aging in non-alcoholic fatty liver disease: Comparison with telomere-specific quantitative FISH and p21 immunohistochemistry

Tomoki Nakajima,[1] Toshiaki Nakashima,[1] Yoshihisa Okada,[2] Masayasu Jo,[2] Taichiro Nishikawa,[2] Yasuhide Mitsumoto,[2] Tatsuo Katagishi,[2] Hiroyuki Kimura,[2] Yoshito Itoh,[2] Keizo Kagawa[3] and Toshikazu Yoshikawa[2]

[1]*Department of Medicine, Saiseikai Kyoto Hospital, Nagaoka-kyo City,* [2]*Molecular Gastroenterology and Hepatology, Kyoto Prefectural University of Medicine Graduate School of Medical Science, and* [3]*Fukuchiyama City Hospital, Fukuchiyama, Kyoto, Japan*

Telomere-specific quantitative fluorescent *in situ* hybridization (Q-FISH) accurately evaluates hepatocellular aging on histological sections, but it requires appropriate tissue processing. To establish a more simple method for the assessment of hepatocellular aging, the usefulness of nuclear size measurement was clarified using biopsy liver samples from 64 patients with non-alcoholic fatty liver disease (NAFLD), a model for oxidative stress-associated hepatocellular aging, and 11 control individuals. Relative telomere intensity (RTI) was measured on Q-FISH, and the relative nuclear size (RNS) was calculated as the average nuclear size of the hepatocytes divided by that of lymphocytes. In normal individuals and NAFLD patients, the RTI and RNS were negatively correlated. The degree of nuclear enlargement in NAFLD patients was larger than that in normal individuals with the same telomere length, possibly reflecting telomere-independent senescence. In NAFLD patients with RNS >2.0, the regenerative responses, indicated by the ratio of Ki-67-positive index to serum alanine aminotransferase level, were significantly reduced. The RNS positively correlated with the p21 expression, another marker of senescence. This all indicates that nuclear enlargement progresses in parallel with reduced regenerative responses, telomere shortening, and p21 upregulation. Nuclear size measurement is an effective method for estimation of hepatocellular aging.

Key words: non-alcoholic fatty liver disease, nuclear enlargement, p21 protein, quantitative fluorescent *in situ* hybridization, senescence, telomere

Correspondence: Tomoki Nakajima, MD, Department of Medicine, Saiseikai Kyoto Hospital, 8-Minamihirao, Imazato, Nagaoka-kyo City, Kyoto 617-0814, Japan. Email: tomnaka@silver.ocn.ne.jp

Received 8 July 2009. Accepted for publication 2 November 2009.

Telomere-specific quantitative fluorescent *in situ* hybridization (Q-FISH) is useful to assess the degree of hepatocellular aging in histological sections. To date, we and other researchers have established the relevant experimental protocols for telomere-specific Q-FISH for various human tissues.[1–4] The advantage of this method is that it enables measurement of the telomere length of each cell on archival paraffin tissue sections, whereas the drawback is that it needs appropriate tissue fixation before staining,[5] strict temperature adjustment during the staining procedure, requirement of immediate result assessment before fluorescent fading, and laboratory equipment with computer-linked fluorescent microscopy for digital quantification. Due to these issues, Q-FISH is used for clinical research only in a limited number of institutions.

The nuclear size of hepatocytes was previously demonstrated to increase progressively along with nuclear DNA polyploidization.[6–8] This alteration is regarded as an age-related process, because polyploid hepatocytes appear in individuals from 1–5 years old, slowly accumulate up to the age of 50 years, and subsequently increase rapidly. Furthermore, as shown in a fibroblast cell line, the level of oxidized bases accumulated in the nuclei is suspected to induce failure in chromatin assembling, also leading to senescence-related nuclear enlargement.[9] It is not clearly understood, however, whether nuclear enlargement progresses in parallel with the telomere shortening process and upregulation of other markers of senescence.

Replicative senescence, classically regarded to be triggered by telomere shortening, could be *p53* dependent, possibly because *p53* detects a disrupted telomeric end structure (the T-loop) or the end-to-end fusion of chromosomes that result from telomere dysfunction.[10] Indeed, p53 activity and

expression of *p21*, a *p53* target gene, increase in senescent cells.[11] In human fibroblasts, because targeted deletion of the *p21* gene is sufficient to bypass senescence, p21 may have a major role in the induction of cellular senescence by suppressing the activity of cyclin-dependent kinases (Cdk).[12] Recent studies have shown that cellular senescence is induced not only by the classical mechanism via the p53/p21 pathway through telomere shortening, but also by activation of the p53/p21 or p16/pRB pathway through various oxidative stresses even before telomeres are critically shortened, the phenomenon so-called 'premature senescence'.[13]

Using telomere-specific Q-FISH, we previously showed that telomere shortening is accelerated in non-alcoholic fatty liver disease (NAFLD), possibly through oxidative stress-induced DNA damage.[14] NAFLD, however, is a heterogeneous disease entity involving a broad spectrum of histopathological states, which is difficult to fully understand in single hospital-based research. To extend our research into a large-scale multi-centered study using many archival tissues stocked at multiple institutions, it is relevant to use a simple method that is not easily influenced by tissue processing conditions such as paraffin embedding, strict temperature conditions, and fluorescent fading effect. Towards this end, we attempted to validate the usefulness of nuclear size measurement for the assessment of hepatocellular aging in terms of reduced regenerative response, telomere shortening, and upregulation of p21 protein.

MATERIALS AND METHODS

Patients

Sixty-four patients (38 male, 26 female) diagnosed with NAFLD in 2003–2006 were selected from the files of the Department of Surgical Pathology of Kyoto Prefectural University of Medicine. Each liver biopsy specimen was diagnosed in a blinded manner by two hepatologists (T.N. and T.N.), according to the histopathological criteria summarized by attendees of the AASLD (American Association for the Study of Liver Diseases) Single Topic Conference 2002.[15] Patients with a history of alcoholism (consuming >20 g/day), showing evidence of hepatitis B or C infection, or taking known hepatotoxic drugs were excluded from the study. Serum alanine aminotransferase (ALT) levels of those patients at the time of biopsy were reviewed from their clinical charts.

Tissue preparation

A total of 64 paraffin-embedded liver tissue biopsies were selected. Eleven histologically normal liver tissues obtained by partial hepatectomy for metastatic liver tumors from patients without NAFLD, and who were negative for hepatitis B surface antigen and anti-hepatitis C antibody, were selected as controls. Informed consent for usage of these tissues for the present study was obtained from all patients in written form.

Of four sections (5 μm each) cut serially from each paraffin block, one each was used for HE staining, immunohistochemistry for Ki-67 antigen and p21 protein, or telomere-specific Q-FISH combined with 4′-6-diamidino-2-phenylindole (DAPI) staining. Various pathological features of NAFLD were semi-quantitatively evaluated based on the scoring system proposed for NAFLD activity score (NAS).[16] Namely, steatosis was scored as 0–3, ballooning as 0–2, and the presence or absence of glycogenated nuclei was scored as 0 or 1. The degree of hepatocellular injury was scored as grades 1, 2 or 3, and the degree of fibrosis was graded as stages 0, 1, 2, 3 or 4, based on the standards proposed by Brunt *et al.*[17]

Telomere-specific quantitative fluorescence *in situ* hybridization

The combined length of telomeres within single cells was determined by the intensity of fluorescence on telomere-specific FISH of each paraffin section, using a Telomere Detection Kit (Dako, Copenhagen, Denmark), as reported previously.[4,14] Image-processed telomeric signals were quantified from digitized fluorescence microscopy images using the image analysis software package IP Laboratories (version 3.54, Scanalytics, Fairfax, VA, USA).

As reported previously, three different cell populations were distinguishable by their morphological features following DAPI staining of each Q-FISH section and HE staining of each serial section.[18] Hepatocytes had round nuclei and a large area of cytoplasmic space. Stellate cells were recognized as elongated cells with elongated nuclei. Lymphocytes were characterized by round nuclei and very little cytoplasm. Lymphocytes, which maintain relatively stable telomere lengths, especially in adults aged ≥40 years, were used as measures for the normal-length telomere fluorescence signal intensity within each tissue sample. Telomere erosion of lymphocytes is reported to be only 1.68 kb from age 40–80 years and 2.00 kb from age 20–40 years.[19]

Telomeric pixel intensities of individual hepatocyte and lymphocyte nuclei were recorded. To control for different amounts of DNA in the sectioned nuclei, the telomeric signal intensity was adjusted by dividing each telomere fluorescence sum for a given nucleus by the sum of the pixels of the DAPI signal within that nucleus, as reported previously. For each field of view, the adjusted telomeric signal intensities of each hepatocyte nucleus and lymphocyte nucleus were designated as Tel-H and Tel-L, respectively. The ratio of mean

Tel-H/mean Tel-L was calculated for each field of view after assessing 15–20 hepatocytes and >10 lymphocytes. Relative telomere intensity (RTI) was defined as the mean of the Tel-H/Tel-L ratios measured from at least five different fields of view per sample under various histological conditions.

Image cytometry of nuclear size

When the fluorescent intensities of hepatocytes and lymphocytes were measured, their nuclear sizes were also simultaneously recorded by IP Laboratories using digital images of DAPI staining. Relative nuclear size (RNS) was calculated by dividing the average nuclear size of hepatocytes (NS-H) by the average nuclear size of lymphocytes (NS-L).

Among the NAFLD patients, those with RNS ≤2.0 were classified as the normo-nucleus group, and those with RNS >2.0 were classified as the enlarged-nucleus group.

To minimize the effect of intralobular heterogeneity of nuclear size, we measured the RTI and RNS of hepatocytes evenly in zones 1, 2 and 3. In addition, the digitized data of both telomeric signal intensity and nuclear size were acquired from the same hepatocyte by adjusting the appropriate fluorescent filters and using IP Laboratories software.

Immunohistochemistry for Ki-67 antigen and p21 protein

Immunohistochemistry for Ki-67 antigen and p21 protein was performed using the streptavidin–biotin–peroxidase complex method, following the manufacturer's instructions. Primary antibodies used were mouse anti-Ki-67 antigen monoclonal antibody (MIB-1; Dako USA, Carpinteria, CA, USA), and mouse anti-p21 monoclonal antibody (SX118; Dako USA). The sections were counterstained with hematoxylin. Negative control slides without the primary antibody were included for each procedure. The Ki-67-positive index and p21-positive index (Ki-67-PI and p21-PI, respectively) were calculated from a minimum of 1000 scored hepatocytes.

As previously reported, we used the Ki-67-PI as an indicator of reactive hepatocyte proliferative activity, and ALT as a measure of necroinflammatory activity.[14] By calculating the relative ratio of Ki-67-PI to ALT from a given sample, we could quantify the replicative response to liver cell injury. Because the frequency of apoptotic hepatocytes was very low, we considered it inappropriate to use apoptotic index to evaluate the degree of cell death in small biopsy specimens.

Statistical analysis

Comparison of the RNS of NAFLD patients and the expected RNS of normal individuals was performed using Wilcoxon's matched-pairs test. Comparison of the ratios of Ki-67-PI to ALT between normo-nucleus and enlarged-nucleus groups was performed using Mann–Whitney *U*-test. Correlation between pathological variables (the degrees of steatosis, ballooning, and Brunt's stages and grades) and RTI, p21-PI, or RNS was assessed on Kruskal–Wallis test. The difference in RTI, p21-PI, and RNS values according to presence or absence of glycogenated nuclei was tested on Mann–Whitney *U*-test. $P < 0.05$ was considered significant.

RESULTS

Histological findings

Hepatocyte injury was scored 1 in three cases, 2 in 13 cases, 3 in 16 cases, 4 in 20cases, 5 in seven cases, 6 in four cases, and 7 in one case, according to NAS. Fibrosis was staged 0 in 27 cases, 1 in 17 cases, 2 in eight cases, and 3–4 in 12 cases, according to the staging system proposed by Brunt *et al.*

Nuclear size and telomere length

The RTI and RNS in normal individuals were 1.101 ± 0.435 and 1.648 ± 0.235, respectively. The microphotograph of a representative example is shown in Fig. 1(a). The RTI and RNS in NAFLD were 0.845 ± 0.287 and 2.116 ± 0.466, respectively. The microphotograph of a representative NAFLD example is shown in Fig. 1(b). The microphotographs of representative nuclear staining by DAPI of lymphocytes Fig. 1(c) and hepatocytes Fig. 1(d), at the same magnification, are shown. In addition, these images were overlaid with the images of telomere FISH visualized with fluorescein isothiocyanate of lymphocytes Fig. 1(e) and hepatocytes Fig. 1(f).

In both normal individuals and NAFLD patients, RTI and RNS were negatively correlated (Fig. 2). Therefore, nuclear size measurement can estimate the degree of telomere reduction in both groups. The degree of nuclear enlargement, however, in most NAFLD patients was larger than that in normal individuals with the same telomere length. The RNS of NAFLD patients was compared with the best-fit RNS of normal individuals with the same RTI predicted by Fig. 2(a). The RNS of NAFLD patients was significantly higher than the predicted normal RNS ($P < 0.001$, Wilcoxon's matched-pairs test; Fig. 3). This result indicates that in NAFLD, hepatocellular senescence progresses even before telomeres are critically shortened.

In normal individuals, RNS and ages were positively correlated (Fig. 4a), indicating that hepatocellular senescence occurs normally during aging. In NAFLD patients there was no correlation between RNS and age (Fig. 4b). The RNS of NAFLD patients was compared with the best-fit RNS of

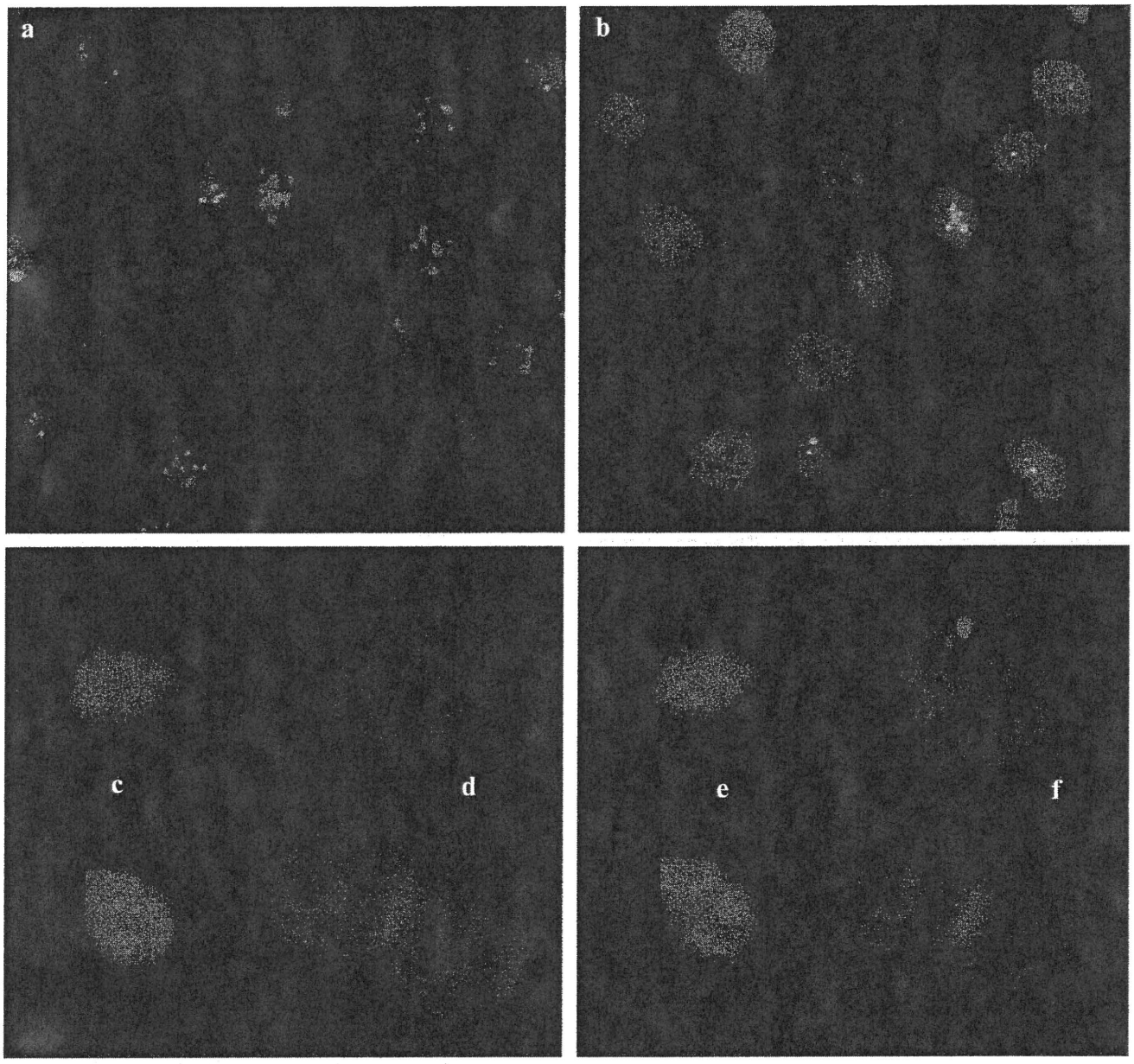

Figure 1 Telomere-specific quantitative fluorescent *in situ* hybridization (Q-FISH) in liver samples. (**a**) Normal individual. Man, 29 years old. The relative telomere intensity (RTI) and relative nuclear size (RNS) were 1.633 and 1.440, respectively. (**b**) Non-alcoholic fatty liver disease (NAFLD) patient (male, 36 years old). The RTI and RNS were 0.678 and 2.096, respectively. The microphotographs of representative nuclear staining by DAPI of (**c**) lymphocytes and (**d**) hepatocytes, at the same magnification, are shown. In addition, these images were overlaid with the images of telomere FISH visualized by fluorescein isothiocyanate of (**e**) lymphocytes and (**f**) hepatocytes.

normal individuals of the same age predicted by Fig. 4(a). The RNS of NAFLD patients was significantly higher than predicted normal RNS ($P < 0.001$, Wilcoxon's matched-pairs test; Fig. 5). This indicates that in NAFLD, nuclear enlargement progresses regardless of age.

Because each cell was double-stained with telomere FISH and DAPI, the correlation between telomere intensity and nuclear size in each nucleus could be determined using representative NAFLD liver specimens. In each microscope field, the adjusted telomere intensity and nuclear size tended to be negatively correlated. A representative example is shown in Fig. 6.

Nuclear size and replicative response

The Ki-67-PI and ALT were closely correlated in the normo-nucleus group (Fig. 7a) and also in the enlarged-nucleus

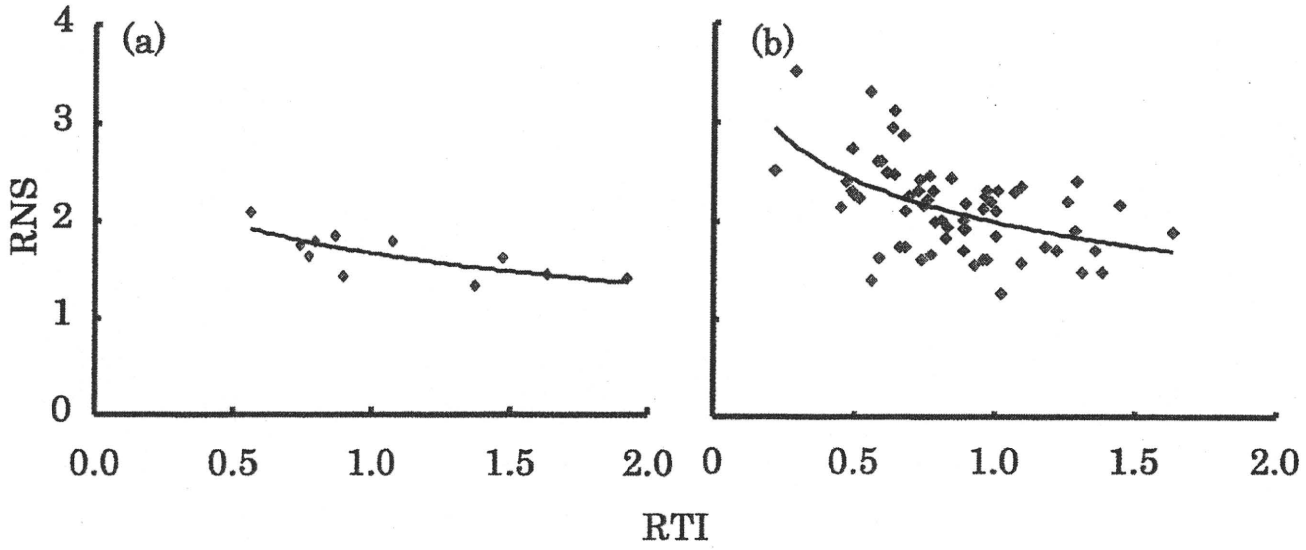

Figure 2 Relationship between relative telomere intensity (RTI) and relative nuclear size (RNS). RTI and RNS were negatively correlated in both (**a**) normal individuals ($y = -0.4681\ln(x) + 1.6606$, $R^2 = 0.5746$, $n = 11$, $P < 0.05$) and (**b**) non-alcoholic fatty liver disease (NAFLD) patients ($y = -0.6431\ln(x) + 1.9752$, $R^2 = 0.2611$, $n = 64$, $P < 0.01$).

group of NAFLD patients (Fig. 7b). The regression lines for Ki-67-PI versus ALT in the normo-nucleus and enlarged-nucleus groups were calculated to be $y = 0.0291x + 1.165$ ($R^2 = 0.449$, $P < 0.001$, $n = 29$) and $y = 0.0136x + 1.530$ ($R^2 = 0.396$, $P < 0.001$, $n = 35$), respectively. The regression slopes of the enlarged-nucleus normo-nucleus groups were significantly different (d.f. = 60, $t = 2.54$, $P < 0.05$).

The ratio of Ki-67-PI to ALT in the enlarged-nucleus group was significantly lower than that in the normo-nucleus group ($P < 0.005$, Mann–Whitney *U*-test), again suggesting that the hepatocellular replicative response of the enlarged-nucleus group is depressed relative to the normo-nucleus group (Fig. 8).

p21 protein expression and telomere shortening

There was a negative correlation between p21-PI and RTI ($R^2 = 0.180$, $P < 0.01$; Fig. 9a), which suggested that telomere shortening may trigger p21 activation, resulting in senescence.

Nuclear size and p21 protein expression

Because replicating hepatocytes in the G2 phase also may manifest nuclear enlargement, it was determined whether nuclear size in NAFLD patients was related to p21 expression, another marker of senescence. As a result, RNS was found to be positively correlated with p21-PI ($R^2 = 0.0781$, $P < 0.05$, Fig. 9b).

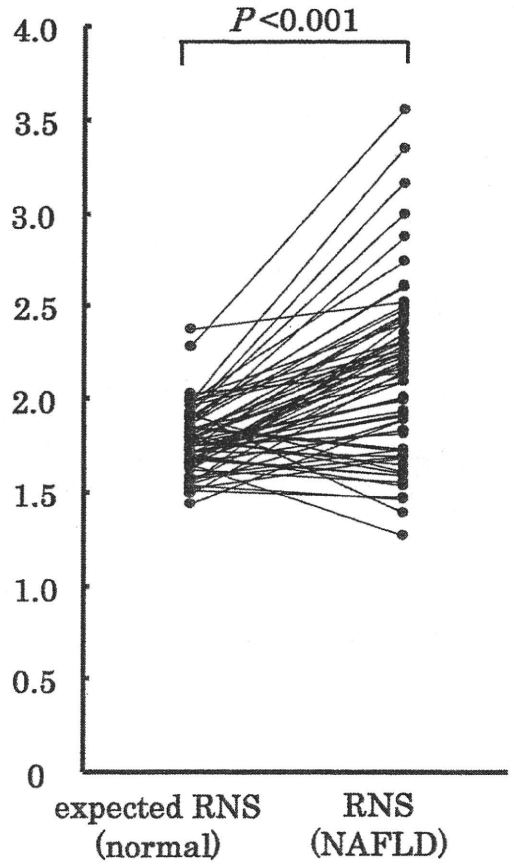

Figure 3 The actual relative nuclear size (RNS) of non-alcoholic fatty liver disease (NAFLD) patients and the expected RNS of normal individuals with the same relative telomere intensity (RTI), which was predicted in Fig. 2(a). The RNS of NAFLD patients was significantly higher ($P < 0.001$, Wilcoxon's matched-pairs test) than the expected value, suggesting that some hepatocytes undergo senescence before telomeres become critically shortened.

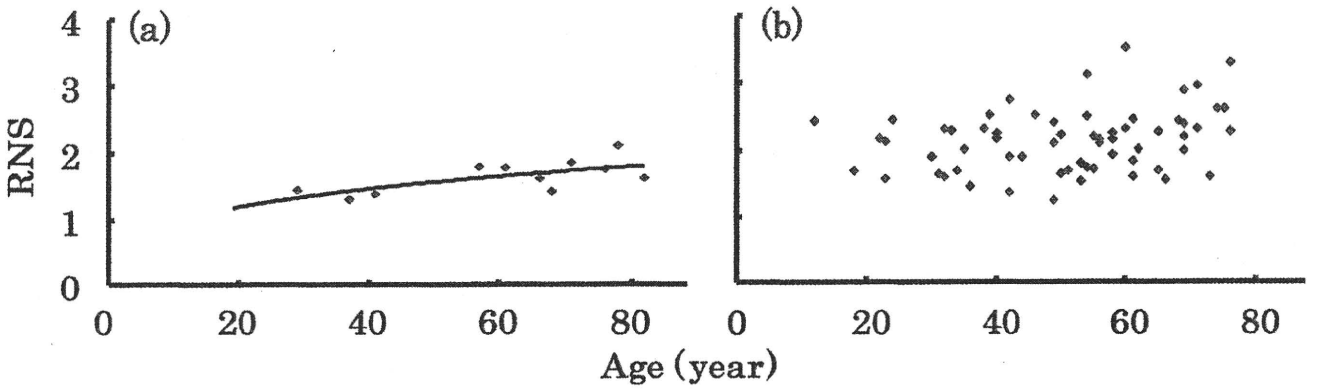

Figure 4 (**a**) In normal individuals, relative nuclear size (RNS) and age was positively correlated ($y = 0.5093x^{0.2873}$, $R^2 = 0.4779$, $n = 11$, $P < 0.05$). (**b**) In non-alcoholic fatty liver disease (NAFLD) patients, there was no correlation between RNS and age ($n = 64$).

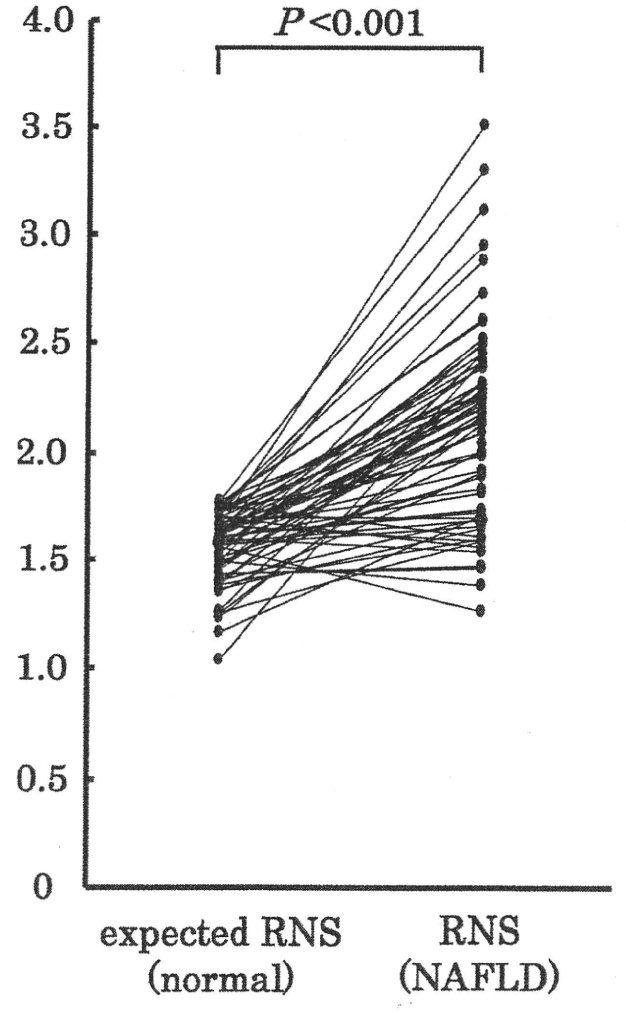

Figure 5 The actual relative nuclear size (RNS) non-alcoholic fatty liver disease (NAFLD) patients and the expected RNS of normal individuals of the same age, which was predicted in Fig. 4(a). The RNS of NAFLD patients was significantly higher ($P < 0.001$, Wilcoxon's matched-pairs test) than the expected values, suggesting that nuclear enlargement progresses irrespective of age.

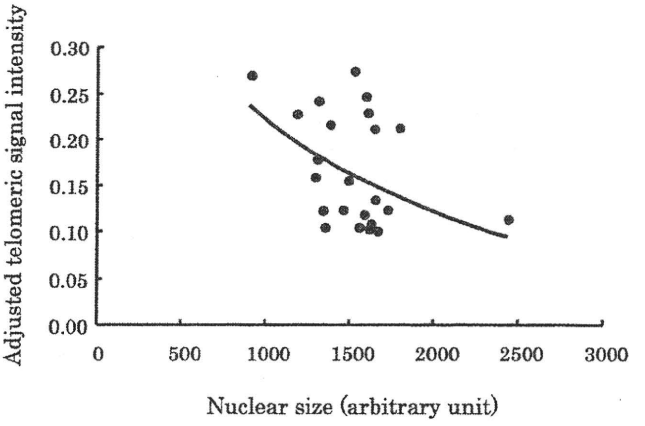

Figure 6 In a representative non-alcoholic fatty liver disease (NAFLD) liver specimen, adjusted telomere intensity and nuclear size were negatively correlated ($y = -0.14671\text{Ln}(x) + 1.239$, $R^2 = 0.179$, $n = 25$, $P < 0.05$).

Relation between pathological changes in NAFLD livers and morphologically aging features

The grade of ballooning correlated negatively with RTI and positively with p21-PI. The degree of fibrosis, assessed using the Brunt *et al.* system, also correlated negatively with RTI and positively with p21-PI. The median RNS was higher in the groups with more advanced fibrosis, but the correlation was not significant. The degree of inflammation, assessed on Brunt grade, was negatively correlated with RTI. The median p21-PI was lower in the groups with more active inflammation. The degree of steatosis and glycogenated nuclei did not significantly correlate with any aging features (Table 1).

DISCUSSION

It is well-known that the nuclear enlargement of hepatocytes progresses as a result of DNA polyploidization.[6–8] A previous

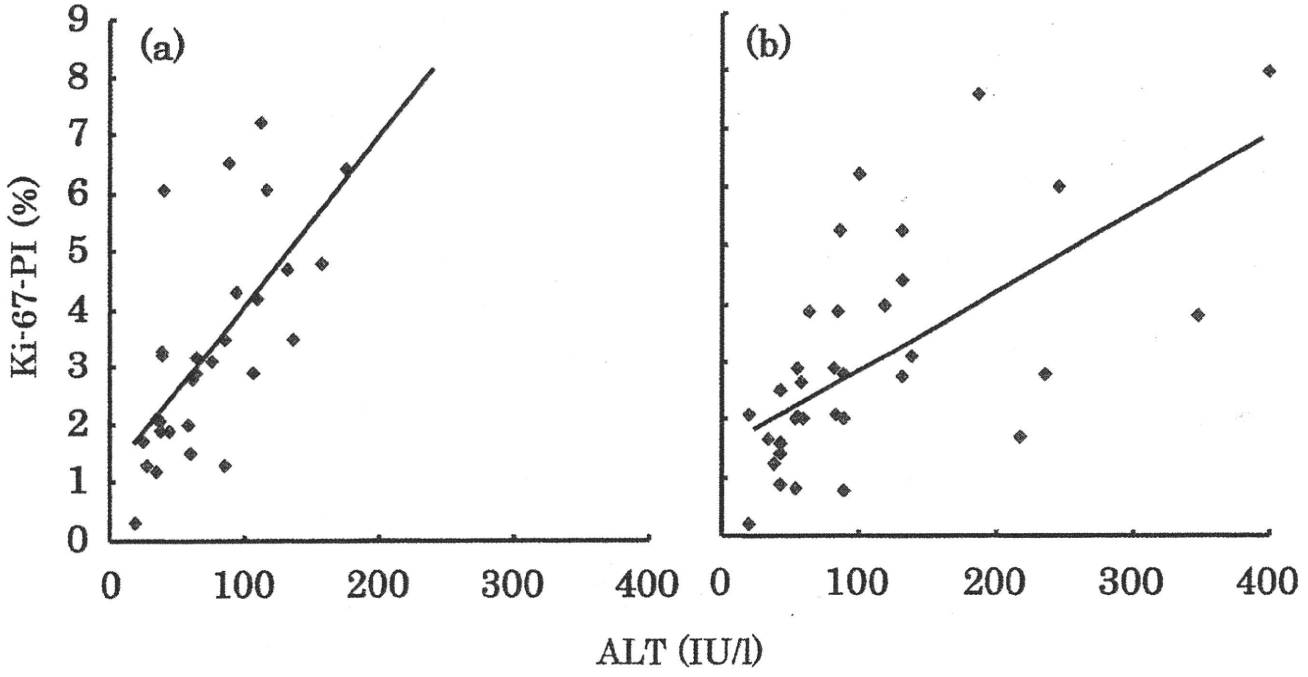

Figure 7 Ki-67-positive index (PI) and serum alanine aminotransferase (ALT) were closely correlated in (**a**) the normo-nucleus group ($y = 0.0291x + 1.165$, $R^2 = 0.449$, $n = 29$) and also in (**b**) the enlarged-nucleus group ($y = 0.0136x + 1.530$, $R^2 = 0.396$, $n = 35$). The regression slopes of the enlarged-nucleus and normo-nucleus groups were significantly different (d.f. = 60, $t = 2.54$, $P < 0.05$).

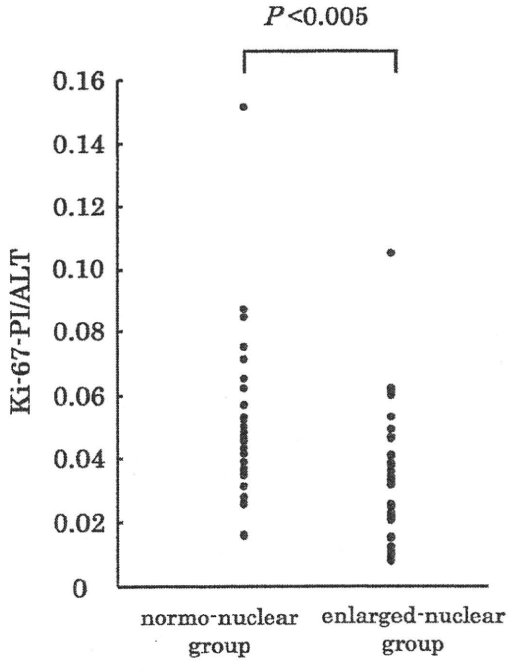

Figure 8 The ratios of Ki-67-positive index (PI) to serum alanine aminotransferase (ALT) of the enlarged-nucleus group were significantly lower than those of the normo-nucleus group ($P < 0.005$, Mann–Whitney *U*-test), suggesting that the hepatocellular replicative response of the enlarged-nucleus group was depressed relative to the normo-nucleus group.

report showed that oxidative DNA damage increases susceptibility for hepatic polyploidy.[20] Oxidative stress-induced DNA injury is also reported to accelerate telomere shortening in addition to the classical telomeric reduction through cell-cycle turnover.[21] In light of these reports, we speculate that, in addition to telomeric reduction through cell-cycle turnover, the chronic oxidative stress, which plays a crucial role in the progression of NAFLD, might be an essential cause for the accelerated telomere shortening, in parallel with the increase in nuclear enlargement from early in life.

The present study showed that average nuclear size and telomere length were negatively correlated in both normal individuals and NAFLD patients. The actual degree of nuclear enlargement in NAFLD patients, however, was significantly larger than that expected in normal individuals of the same telomere length. These results indicate that in NAFLD, some hepatocytes undergo senescence before telomeres are critically shortened. This telomere shortening-independent senescence may be due to chronic exposure of oxidative stress to hepatocytes, as previously reported in basic experimental cell research.[22–24] Furthermore, the previous reports that 8-hydroxy-2′-deoxyguanosine, a marker of oxidative DNA damage, is expressed in varying degrees in NAFLD livers, but not in the normal livers,[25] also support the mechanism of senescence induced by oxidative stress.

In addition to being an important contributor to senescence, oxidative stress was suggested to morphologically

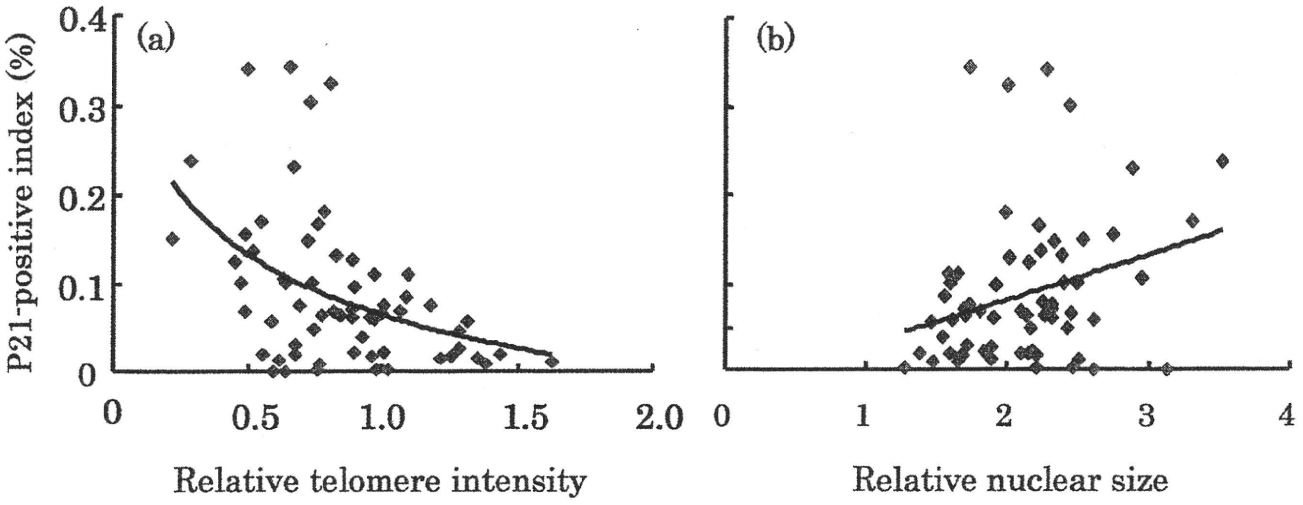

Figure 9 In non-alcoholic fatty liver disease (NAFLD) patients, there was (**a**) a negative correlation between p21-positive index and relative telomere intensity ($y = -0.0955\text{Ln}(x) + 0.0668$, $R^2 = 0.180$, $P < 0.01$), and (**b**) a positive correlation between relative nuclear size and p21-positive index ($y = 0.0502x - 0.0174$, $R^2 = 0.0781$, $P < 0.05$).

Table 1 Pathological features of NAFLD and hepatocellular aging

	Relative telomere intensity		p21-positive index (%)		Relative nuclear size	
Ballooning						
0	0.848		0.062		2.113	
1	0.841	$P = 0.005$	0.070	$P = 0.041$	1.730	$P < 0.001$
2	0.731		0.129		2.385	
Brunt's stage						
0	0.895		0.063		2.097	
1–2	0.770	$P = 0.030$	0.071	$P = 0.036$	2.153	$P = 0.520$
3–4	0.637		0.084		2.249	
Brunt's grade						
1	0.887		0.067		2.202	
2	0.853	$P < 0.001$	0.070	$P = 0.475$	2.006	$P = 0.203$
3	0.758		0.112		2.143	
Steatosis						
1	0.834		0.065		2.225	
2	0.891	$P = 0.490$	0.070	$P = 0.495$	1.916	$P = 0.387$
3	0.758		0.112		2.143	
Glycogenated nuclei						
0	0.944		0.056		2.147	
1	0.813	$P = 0.337$	0.072	$P = 0.398$	2.136	$P = 0.908$

cause ballooning of hepatocytes.[26] In the present study, this was supported by the tendency toward higher grade of ballooning in aging hepatocytes. Furthermore, the stage of fibrosis was increased in parallel with hepatocellular aging, which is compatible with the accepted notion that fibrosis progression is the result of cell-cycle turnover of hepatocytes[18] and accelerated by oxidative stress,[27] both of which are associated with hepatocellular aging.

We determined that the enlarged-nucleus group had a lower replicative response to necroinflammation than the normo-nucleus group, which possibly reflects one of the features of hepatocellular senescence. To date, two inhibitors of Cdk, p21 and p16, have been known to play an important role in irreversible cell-cycle arrest in senescent cells.[13] In the present study we showed that p21 expression was increased in parallel with nuclear enlargement, suggesting that p21 suppresses cell-cycle turnover by binding to and inactivating most cyclin-Cdk complexes in the hepatocytes in NAFLD.[28] In addition, we preliminarily attempted to determine p16 expression on immunohistochemistry using mouse anti-human p-16 protein, clone E6H4 (Dako, Copenhagen, Denmark), as a primary antibody as per the manufacturer's instruction. p16 immunopositivity, however, was not observed in the hepatocytes in any of the present biopsy samples. Because some researchers have reported p16 expression in hepatocytes in diseased livers using primary antibodies of

different clones,[29,30] further studies on the reactivity of different anti-p16 antibodies under various antigen retrieval methods are warranted.

From a technical viewpoint, the problem with Q-FISH is that the result is especially affected by the duration and kinds of tissue fixation.[5] Therefore, in a multi-centered study using archival tissues stocked at multiple institutions, the variable conditions of tissue processing can influence the results. In contrast, nuclear size is measurable using HE-stained archival tissue specimens, and is not easily influenced by the differences in tissue processing conditions before staining. In the present study, the validity of this simple method has been demonstrated for the assessment of hepatocellular aging in NAFLD.

REFERENCES

1 Meeker AK, Gage WR, Hicks JL *et al.* Telomere length assessment in human archival tissues: Combined telomere fluorescence in situ hybridization and immunostaining. *Am J Pathol* 2002; **160**: 1259–68.
2 Ferlicot S, Youssef N, Feneux D, Delhommeau F, Paradis V, Bedossa P. Measurement of telomere length on tissue sections using quantitative fluorescence in situ hybridization (Q-FISH). *J Pathol* 2003; **200**: 661–6.
3 Kapoor V, Telford WG. Telomere length measurement by fluorescence in situ hybridization and flow cytometry. *Methods Mol Biol* 2004; **263**: 385–98.
4 Nakajima T, Katagishi T, Moriguchi M *et al.* Tumor size-independence of telomere length indicates an aggressive feature of HCC. *Biochem Biophys Res Commun* 2004; **325**: 1131–5.
5 Hepperger C, Otten S, von Hase J, Dietzel S. Preservation of large-scale chromatin structure in FISH experiment. *Chromosoma* 2007; **116**: 117–33.
6 Watanabe T, Shimada H, Tanaka Y. Human hepatocytes and aging: A cytophotometrical analysis in 35 sudden-death cases. *Virchows Arch B Cell Pathol* 1978; **27**: 307–16.
7 Watanabe T, Tanaka Y. Age-related alterations in the size of human hepatocytes. A study of mononuclear and binuclear cells. *Virchows Arch B Cell Pathol* 1982; **39**: 9–20.
8 Kudryavtsev BN, Kudryavtseva MV, Sakuta GA, Stein GI. Human hepatocyte polyploidization kinetics in the course of life cycle. *Virchows Arch B Cell Pathol* 1993; **64**: 387–93.
9 Mocali A, Giovannelli L, Dolora P, Paoletti F. The comet assay approach to senescent human diploid fibroblasts identifies different phenotypes and clarifies relationships among nuclear size, DNA content, and DNA damage. *J Gerontol A Biol Sci Med Sci* 2005; **60**: 695–701.
10 Itahana K, Dimri GP, Hara E *et al.* A role for p53 in maintaining and establishing the quiescence growth arrest in human cells. *J Biol Chem* 2002; **277**: 18206–14.
11 Noda A, Ning Y, Venable SF, Pereira-Smith OM, Smith JR. Cloning of senescent cell-derived inhibitors of DNA synthesis using an expression screen. *Exp Cell Res* 1994; **21**: 90–98.
12 Brown JP, Wei W, Sedivy JM. Bypass of senescence after disruption of p21 CIP1/WAF1 gene in normal diploid human fibroblasts. *Science* 1997; **277**: 831–4.
13 Itahana K, Campisi J, Dimri GP. Mechanisms of cellular senescence in human and mouse cells. *Biogerontology* 2004; **5**: 1–10.
14 Nakajima T, Moriguchi M, Katagishi T *et al.* Premature telomere shortening and impaired regenerative response in hepatocytes of individuals with NAFLD. *Liver Int* 2006; **26**: 23–31.
15 Neuschwander-Tetri BA, Caldwell SH. Nonalcoholic steatohepatitis: Summary of an AASLD conference. *Hepatology* 2003; **37**: 1202–19.
16 Kleiner DE, Brunt EM, van Natta M *et al.* Design and validation of a histological scoring system for nonalcoholic fatty liver disease. *Hepatology* 2005; **41**: 1313–21.
17 Brunt EM, Janney CG, Di Bisceglie AM, Neuschwander-Tetri BA, Bacon BR. Nonalcoholic steatohepatitis: A proposal for grading and staging the histological lesions. *Am J Gastroenterol* 1999; **94**: 2467–74.
18 Wiemann SU, Satyanarayana A, Tsahuridu M *et al.* Hepatocyte telomere shortening and senescence are general markers of human liver cirrhosis. *FASEB J* 2002; **16**: 935–42.
19 Iwama H, Ohyashiki K, Ohyashiki JH *et al.* Telomeric length and telomerase activity vary with age in peripheral blood cells obtained from normal individuals. *Hum Genet* 1998; **102**: 397–402.
20 Gorla GR, Malhi H, Gupta S. Polyploidy associated with oxidative injury attenuates proliferative potential of cells. *J Cell Sci* 2001; **114**: 2943–51.
21 von Zgliniki T. Oxidative stress shortens telomeres. *Trends Biochem Sci* 2002; **27**: 330–44.
22 Toussaint O, Remacle J, Dierick JF *et al.* From the Hayflick mosaic to the mosaics of ageing. *Int J Biochem Cell Biol* 2002; **34**: 1415–29.
23 Kurz DJ, Decary S, Hong Y, Trivier E, Akhmedov A, Erusalimsky JD. Chronic oxidative stress compromises telomere integrity and accelerates the onset of senescence in human endothelial cells. *J Cell Sci* 2004; **117**: 2417–26.
24 Ohshima S. Abnormal mitosis in hypertetraploid cells causes aberrant nuclear morphology in association with H_2O_2-induced premature senescence. *Cytometry A* 2008; **73**: 808–15.
25 Seki S, Kitada T, Yamada T, Sakaguchi H, Nakatani K, Wakasa K. In situ detection of lipid peroxidation and oxidative DNA damage in non-alcoholic fatty liver diseases. *J Hepatol* 2002; **37**: 56–62.
26 Lackner C, Gogg-Kamerer M, Zatloukal K, Stumptner C, Brunt EM, Denk H. Ballooned hepatocytes in steatohepatitis: The value of keratin immunohistochemistry for diagnosis. *J Hepatol* 2008; **48**: 821–8.
27 Sekoguchi S, Nakajima T, Moriguchi M *et al.* Role of cell-cycle turnover and oxidative stress in telomere shortening and cellular senescence in patients with chronic hepatitis C. *J Gastroenterol Hepatol* 2007; **22**: 182–90.
28 Sherr CJ, Roberts JM. CDK inhibitors: Positive and negative regulators of G1-phase progression. *Genes Dev* 1999; **13**: 1501–12.
29 Plentz RR, Park YN, Lechel A *et al.* Telomere shortening and inactivation of cell cycle checkpoints characterize human hepatocarcinogenesis. *Hepatology* 2007; **45**: 968–76.
30 Kim H, Oh B-K, Roncalli M *et al.* Large liver cell change in hepatitis B virus-related liver cirrhosis. *Hepatology* 2009; **50**: 752–62.

Laboratory Investigation (2010), 1–10

Blockade of interleukin-6 signaling enhances hepatic steatosis but improves liver injury in methionine choline-deficient diet-fed mice

Kanji Yamaguchi[1], Yoshito Itoh[1], Chihiro Yokomizo[1], Takeshi Nishimura[1], Toshihisa Niimi[1], Hideki Fujii[1], Takeshi Okanoue[1,2] and Toshikazu Yoshikawa[1]

Inflammatory processes have an important role in the development of hepatic steatosis and progression to non-alcoholic steatohepatitis (NASH). Interleukin-6 (IL-6) is known to be a proinflammatory cytokine, but also promotes liver regeneration and protects the liver against various forms of damage. The role of IL-6/Glycoprotein130 (GP130) in NASH remains unclear. In this study, we determined whether blocking IL-6/GP130 signaling prevents progression of steatohepatitis in a mouse NASH model. Six-week-old male C57/BL6 mice were fed either chow control or a methionine choline-deficient (MCD) diet for 8 weeks. Half of the MCD diet-fed mice were treated with 15 mg/kg rat anti-mouse IL-6 receptor antibody (MR16-1), intraperitoneally twice weekly, the remainder and chow-fed mice were injected with 15 mg/kg rat IgG as a control. Hepatic steatosis, injury, fibrosis, apoptosis, markers of lipid peroxidation/oxidant stress and IL-6-related gene expressions were evaluated. MR16-1 treatment decreased signal transducer and activator of transcription 3 activities and expression of suppressor of cytokine signaling 3 in MCD diet-treated mouse livers. Although this treatment enhanced intrahepatic lipid accumulation accompanied by increased sterol regulatory element-binding protein 1 and decreased peroxisome proliferator-activated receptor-α expression, elevated plasma alanine aminotransferase levels were improved with decreased plasma free fatty acid levels, lipid peroxidation/oxidant stress and hepatic apoptosis. Blocking IL-6/GP130 signaling by MR16-1 enhanced MCD diet-induced hepatic steatosis, but ameliorated liver injury. These findings suggest that hepatic IL-6 signaling has a protective role against the progression of hepatic steatosis but may enhance liver inflammation.

Laboratory Investigation advance online publication, 5 April 2010; doi:10.1038/labinvest.2010.75

KEYWORDS: NASH; IL-6; MCD diet; STAT3; SREBP-1

Nonalcoholic fatty liver disease (NAFLD) is one of the most common liver diseases worldwide.[1] According to the two-hit hypothesis for NAFLD progression, hepatic steatosis is a risk factor for nonalcoholic steatohepatitis (NASH) and fibrosis.[2] Continuous excess triglyceride accumulation induces proinflammatory cytokines, produces reactive oxygen species (ROS) and leads to NASH. Proinflammatory cytokines, such as tumor necrosis factor-alpha (TNF-α) and interleukin (IL)-6, are believed to have a central role in this process. Plasma TNF-α levels have been reported to be higher in patients with NASH than in patients with steatosis and controls with no known liver diseases.[3,4] *In vivo* studies have shown that treatment of leptin-deficient ob/ob mice with antibodies against TNF-α improved NASH and hepatic insulin resistance. Mice genetically deficient in the TNF type 1 receptor were resistant to steatosis and liver injury induced by a high-carbohydrate and a methionine choline-deficient (MCD) diet.[5]

Although cytokine imbalance and, in particular, an increase in TNF-α may have a key role in the development of NASH, the role of IL-6 remains obscure. IL-6 is a cytokine with numerous effects, which are dependent on TNF-α acting as an upstream mediator.[6,7] Previous studies have shown that, despite no significant difference between fatty liver and NASH patients, inflammatory C-reactive protein (CRP) was increased in both liver and adipose tissues in patients with

[1]Molecular Gastroenterology and Hepatology, Graduate School of Medical Science, Kyoto Prefectural University of Medicine, Kyoto, Japan and [2]Center of Gastroenterology and Hepatology, Saiseikai Suita Hospital, Osaka, Japan
Correspondence: Dr Y Itoh, MD, PhD, Department of Molecular Gastroenterology, Kyoto Prefectural University of Medicine, 465 Kajii-cho, Kawaramachi-Hirokoji, Kamigyou-ku, Kyoto 602-8566, Japan.
E-mail: yitoh@koto.kpu-m.ac.jp

Received 28 July 2009; revised 23 December 2009; accepted 11 February 2010; published online 5 April 2010